SUBSECTION 2.4.6: PROBABLE MAXIMUM TSUNAMI HAZARDS TABLE OF CONTENTS

SUBSECTION 2.4.6 LIST OF TABLES

SUBSECTION 2.4.6 LIST OF FIGURES

SUBSECTION 2.4.6 LIST OF FIGURES (CONT.)

2.4.6 PROBABLE MAXIMUM TSUNAMI HAZARDS

PTN COL 2.4-2

This subsection examines the tsunamigenic sources and identifies the probable maximum tsunami (PMT) that could affect the safety-related facilities of Units 6 & 7. It evaluates potential tsunamigenic source mechanisms, source parameters, and resulting tsunami propagation from published studies, and estimates tsunami water levels at the site based on site-specific numerical model simulation results. Historical tsunami events recorded along the Florida coast are reviewed to support the PMT assessment. The approach taken is aligned with the PMT evaluation methodology proposed in NUREG/CR-6966 (Reference 201).

Units 6 & 7 are adjacent to the Biscayne Bay shore approximately 8 miles west of Elliott Key Barrier Island on the coast of the Atlantic Ocean, as shown on Figure 2.4.1-201. The grade elevations at the Units 6 & 7 plant area vary from approximately 19.0 feet to 25.5 feet NAVD 88. The entrance floor elevation of all safety-related structures (also referred to as the design plant grade elevation in the AP1000 DCD, which is 100 feet, or 30.48 meters, in the DCD reference datum) is at elevation 26 feet NAVD 88. The plant area is protected by a retaining wall structure with top elevation of 20.0 feet to 21.5 feet NAVD 88. As the grade is relatively high, tsunami events are not expected to pose any hazard to safety-related structures, systems, and components (SSCs) of Units 6 & 7, as described in the subsections below.

2.4.6.1 Probable Maximum Tsunami

The Atlantic and Gulf of Mexico Tsunami Hazards Assessment Group (AGMTHAG) evaluated potential tsunamigenic source mechanisms that may generate destructive tsunamis and affect the U.S. Atlantic and Gulf of Mexico coasts (Reference 202). The major tsunamigenic sources that may affect the southeastern U.S. coasts can be summarized as follows: submarine landslides along the U.S. Atlantic margin, submarine landslides in the Gulf of Mexico, far-field submarine landslide sources, earthquakes in the Azores-Gibraltar plate boundary, and earthquakes in the north Caribbean subduction zones (referred to as the Caribbean-North American plate boundary in Subsection 2.5.1).

Based on the below descriptions of the different source mechanisms, transoceanic tsunamis as a result of earthquakes in the Azores-Gibraltar (east Atlantic) plate boundary and tsunamis generated in the northeastern Caribbean

region are identified as the primary candidates of the PMT generation that could affect Units 6 & 7.

2.4.6.1.1 Submarine Landslides along the U.S. Atlantic Margin

Submarine landslide zones along the U.S. Atlantic margin are concentrated along the New England and Long Island, New York sections of the margin, outward of major ancient rivers in the mid-Atlantic region, and in the salt dome province offshore of North and South Carolinas, as shown in Figure 2.4.6-201 (Reference 202). Although submarine landslides along the U.S. Atlantic margin, from Georges Bank offshore of the New England coast to Blake Spur south of the Carolina Trough, have the potential to cause devastating tsunamis locally, the presence of a wide continental shelf is expected to reduce their impact at the shoreline near the landslides (Reference 202).

AGMTHAG mapped a total of 48 landslide affected areas based on data compiled from bathymetry, GLORIA (Geological Long-Range Inclined Asdic) sidescan sonar imagery, seismic reflection profiles, and sediment core data (Reference 202). The general characteristics of the mapped landslides are summarized in Table 2.4.6-201. The distribution of landslide locations identified along the U.S. Atlantic margin from the Georges Bank to the Carolina Trough is shown in Figure 2.4.6-202. The largest submarine landslide area near Units 6 & 7 is identified in an area south of Cape Hatteras, off the Carolina Trough. The largest landslide in this area exceeds 15,241 square kilometers (5885 square miles) with a volume in excess of 150 cubic kilometers (36 cubic miles). Tectonic activities of the salt domes have been suggested as the triggering mechanism for the landslides in this area along with suggestions that decomposition of gas hydrates due to sea level change and small shallow earthquakes may also have contributed to the formation of these landslides (Reference 202).

Units 6 & 7 are located approximately 400 miles (640 kilometers) southwest of Blake Spur with a wide and shallow continental slope and shelf in between (Figure 2.4.6-201). Details of the Atlantic continental shelf near the site are described in Subsection 2.5.1.1.1.1. Additionally, the landslide zones are oriented in a manner that Units 6 & 7 would be away from the main axis of submarine landslide-generated tsunamis. Consequently, the impact of any submarine landslide-generated tsunami on the continental slope and shelf north of Blake Spur would be considerably reduced before reaching Units 6 & 7.

Twichell et al. studied submarine erosion and characterized morphologic provinces for the Blake Escarpment (Figure 2.4.6-203) northeast of Units 6 & 7

(Reference 203). The Blake Escarpment, extending approximately 450 kilometers (280 miles) to the south from Blake Spur, is one of the largest cliffs in the ocean with a relief of about 4000 meters (13,120 feet) (Reference 203). Near the southern edge of the escarpment, it crosses with the Jacksonville fracture zone, which underlies the Blake plateau at the location of Abaco Canyon. The escarpment was isolated from the continent-derived sediments since late Cretaceous, first by the currents in the Suwannee Straits and later by the Gulf Stream, and erosion of the escarpment is evident over the period (Reference 203).

Twichell et al. identified three morphologic provinces along the Blake Escarpment with varying erosional behavior (Reference 203). These are (1) valleys with tributary gullies, (2) box canyons, and (3) strait terraces. Valleys with tributary gullies are in the northern part of the escarpment near Blake Spur that have undergone no or very little erosion over time. Box canyons are formed by the differential settlement of base rock probably over a long period and are identified south of the Jacksonville fracture zone. The overlying carbonate strata in box canyons are fragmented with continued erosion. The middle reach of the escarpment has straight terraces formed by differential erosion of lithologic differences in the strata exposed along the cliff faces and has lower erosion potential than box canyons (Reference 203). The study by Twichell et al. identified evidence of debris accumulation at the base of the escarpment; however, it did not characterize any tsunamigenic source in the escarpment (Reference 203). Units 6 & 7 are sheltered by the islands of the Bahamas from tsunamis, if any, generated in the region, thus protecting Units 6 & 7 from being affected by large tsunamis.

The Ocean Drilling Program (ODP) provides stratigraphic information on the Bahama platform and the Straits of Florida from borehole and seismic reflection survey results. The ODP data suggest evidence of significant submarine debris flows and turbidite deposits during a four million year interval in the middle Miocene (Reference 217). However, no stratigraphic evidence could be established to relate these Miocene gravity flows to any tsunami deposit or tsunami-like event along the southern Florida coasts. After the Miocene, no debris flow or turbidite deposit could be identified in this region, possibly due to the erosional effects of the Gulf Loop Current that was first established in the Pliocene. It is hypothesized that the debris flow and turbidite deposit resulted from materials that had accumulated atop the carbonate banks at a marine high stand, which became unstable as sea level fell (Reference 217). Such debris flows are not expected to occur in the recent geological environment of eustatic sea level

rise. Therefore, submarine landslide in the Straits of Florida and Bahamas regions is precluded as a PMT source candidate for the Units 6 & 7 site. Details of stratigraphic information in the Bahamas and the Straits of Florida are provided in Subsection 2.5.1.1.1.2. Potential geological hazards near the site region are described in Subsection 2.5.1.1.5.

Information on submarine landslide along the northern coast of Cuba is very scarce. Iturralde-Vinent (Reference 218) summarizes the current understanding of tsunami hazards in Cuba, details of which are provided in Subsection 2.5.1.1.5. Iturralde-Vinent identifies potential tsunami hazards for the Cuban north coast region based on large carbonate boulders found on marine terraces; however, no submarine landslide zones were identified in this region. Consequently, a submarine landslide along the north coast of Cuba was not included as a candidate PMT source for the Units 6 & 7 site.

Units 6 & 7, therefore, would not be impacted by significant submarine landslide-generated tsunamis from the U.S. Atlantic margin, the straits of Florida, Bahamas, or Cuba regions.

2.4.6.1.2 Submarine Landslides in the Gulf of Mexico

Within the Gulf of Mexico, evidences of submarine landslides are recorded in all three geological provinces (Carbonate, Salt, and Canyon/Fan) (Reference 202). The geological provinces within the Gulf of Mexico are shown in Figure 2.4.6-204. The largest submarine failures are found in the Canyon/Fan Province within the Mississippi Fan that was probably active 7500 years ago. The largest failure in the Salt Province is identified offshore of the Rio Grande River. Landslide evidences in the Carbonate Province are identified in the West Florida and Campeche Escarpments along the eastern and southern Gulf of Mexico, respectively (Reference 202).

Significant landslides on the West Florida Slope above the Florida Escarpment (Figure 2.4.6-205) are sourced in Tertiary and Quaternary carbonate deposit. This landslide zone, which is located approximately 300 miles (480 kilometers) west of Units 6 & 7, is hypothesized to be a composite of at least three generations of failures (Reference 202).

Based on the mapping of landslide zones in the Gulf of Mexico, AGMTHAG identified four likely landslide zones and characterized tsunamigenic source parameters that could be used to calculate corresponding tsunami amplitudes (Reference 202). However, because Units 6 & 7 are located on the eastern side of

the Florida peninsula opposite of the Gulf of Mexico shoreline and a very wide continental shelf exists along the Gulf Coast of Florida, tsunamis generated within the Gulf of Mexico would likely be dissipated before reaching Units 6 & 7. Therefore, it was concluded that landslide-generated tsunamis from the Gulf of Mexico sources would not affect the safety-related facilities of Units 6 & 7 that have a design plant grade elevation of 26 feet NAVD 88.

2.4.6.1.3 Far-Field Submarine Landslide Sources

Ward and Day (Reference 204) postulated a mega-tsunami scenario as a result of a possible catastrophic flank failure of the Cumbre Vieja volcano at La Palma of Canary Islands. They estimated that a future volcanic eruption of Cumbre Vieja could slide up to 500 cubic kilometers (120 cubic miles) of rock volume into the ocean running westward 60 kilometers (37.3 miles) offshore at a speed of 100 meters per second (328 feet per second) resulting in a tsunami amplitude of 20–25 meters (66-82 feet) at the Florida Atlantic coast. However, Mader pointed out that the assumption of linear propagation of shallow water wave, as used in Ward and Day's analysis, only described geometrical spreading of waves and ignored the effects of short period wave dispersion (Reference 205). Such an assumption would overpredict the tsunami amplitude. Using the SWAN computer code, Mader computed a maximum tsunami amplitude less than 3.0 meters (10.0 feet) along the U.S. Atlantic coast and less than 1.0 meter (3.3 feet) near Miami, Florida (Reference 205). Mader adopted the initial tsunami amplitude as obtained from the physical model study of the Cumbre Vieja volcano flank failure performed at the Swiss Federal Institute of Technology (Reference 205). The Swiss Federal Institute of Technology experiment considered the failure as a single monolithic block (Reference 205). Pararas-Carayannis also disputed the claim by Ward and Day that a collapse of the Cumbre Vieja volcano is imminent (Reference 206).

More recent modeling efforts by Gisler et al. of the Cumbre Vieja volcano flank failure also showed significant wave dispersion (Reference 207). From the model simulation results, Gisler et al. demonstrated that the tsunami amplitude decay is proportional to $r^{-1.85}$ and $r^{-1.0}$, where r is the distance from tsunami source, for the two- and three-dimensional models, respectively. The simulated tsunami amplitude varied between 1 and 77 centimeters (0.4 and 30 inches) along the Florida Coast (Reference 207). Gisler et al. used smaller slide volume but much higher slide speed compared to those used in Ward and Day (Reference 202). The amplitude in Ward and Day model scales proportionally with rock volume times slide speed. Hence, the much smaller predicted amplitude of Gisler et al. for the Florida coast cannot be attributed to the smaller slide volume

(Reference 202). AGMTHAG concluded that a tsunami from this source is not expected to cause a devastating tsunami along the east coast of the United States (Reference 202).

The other notable far-field submarine landslide tsunami sources are located along the glaciated margins of northern Europe and Canada (Reference 202). The Storegga landslide in northern European margin is identified as a composite of seven slides over the past one-half million years with the largest and most recent landslide dated at 8150 years before present. The resulting tsunamis affected the coasts of Norway, Faeroes islands, Shetland islands, Scotland and northern England. The impacted areas were all within 600 kilometers (375 miles) of the slide (Reference 202).

The Grand Banks landslide in the Scotian margin near Newfoundland, Canada generated a devastating tsunami locally in 1929 (References 202 and 208). AGMTHAG indicated that increased deposition and slope failure on the Scotian margin was due to glacial advance that reached close to the shelf edge about one-half million years before present. However, deposition rate decreased significantly about 8000 years ago as deglaciation ended (Reference 202). The 1929 Grand Banks landslide is one of the only two landslide occurrences in the Scotian margin postdated to the Holocene. Units 6 & 7 would not be affected by teletsunamis from these landslide sources because the tsunamis would be dissipated before reaching them.

2.4.6.1.4 Earthquakes in the Azores-Gibraltar Plate Boundary

Tsunamigenic earthquake sources that may affect the Florida Atlantic Coast are located west of Gibraltar in the Azores-Gibraltar plate boundary near Portugal in the East Atlantic Ocean (at the Africa-Eurasia plate boundary) and in the northeastern Caribbean Basin (Caribbean-North American plate boundary). The Azores-Gibraltar plate boundary separates the African and Eurasian plates, as shown in Figure 2.4.6-206, and has been identified as the source of the largest earthquakes and tsunamis in the north Atlantic basin (Reference 202). AGMTHAG summarized six large tsunamigenic earthquakes that had occurred in this region over the past 300 years—in 1722, 1755, 1761, 1941, 1969 and 1975 (Reference 202). The 1755 Great Lisbon Earthquake, which was estimated in earthquake moment magnitude (M_w) to be 8.5–9.0, had the largest documented felt area of any shallow water earthquake in Europe, and was the largest natural disaster to have affected Europe in the past 500 years (Reference 202). The earthquake motion and ensuing submarine landslide contributed to tsunami waves of 5 to 15 meters (16.4 to 49.2 feet) that devastated the coasts of

southwest Iberia and northwest Morocco and were reported as far north as Cornwall, England (Reference 202). Figure 2.4.6-206 shows the general tectonic setting and bathymetry of the eastern segment of the Azores-Gibraltar plate boundary.

The large tsunami waves also travelled across the Atlantic reaching as far north as Newfoundland, Canada and as far south as Brazil, and caused widespread damage in the eastern Lesser Antilles (Reference 202). However, there is no record of tsunami run-up on the U.S. east coast from this event, although several populated cities existed along the U.S. Atlantic coast in 1755 (Reference 202). Computer simulations by Mader (Reference 209) indicated that the maximum tsunami amplitude including run-up in the U.S. east coast was approximately 3.0 meters (10.0 feet). AGMTHAG simulated the 1755 earthquake tsunami with the source location varying within the Azores-Gibraltar region. The maximum tsunami amplitude in the deep water along the U.S. Atlantic margin was obtained as approximately 0.6 meter (2.0 feet) for a tsunami source location east of the Madeira Tore Rise (Figure 5-8, Reference 202). Further discussion of the 1755 earthquake-generated tsunami is provided in Subsections 2.4.6.2 and 2.4.6.3.

2.4.6.1.5 Earthquakes in the North Caribbean Subduction Zones

The Caribbean region is characterized by high seismic activities and is associated with a large number of past tsunamis (References 210 and 211). Tsunami sources in the northeastern Caribbean Basin that may affect the Florida Atlantic coast include the Puerto Rico and Hispaniola trenches, as shown in Figure 2.4.6-207. AGMTHAG simulated the distribution of peak offshore tsunami amplitude along the Gulf of Mexico and Atlantic Coasts from a postulated earthquake in the Puerto Rico trench. The simulation, which used a linear long-wave model for the deepwater regions and did not include frictional effects, predicted the maximum tsunami amplitude to be no more than 0.1 meter (0.3 foot) at a water depth of 250 meters (820 feet) near the longitude of approximately 80.2° W (longitude position estimated from Figure 8-2c of Reference 202). This longitude position represents generally the location within the Straits of Florida, which is south-southwest of Units 6 & 7. The maximum deepwater tsunami amplitudes along the U.S. Atlantic coast, however, were much higher, close to 5 meters (16.4 feet) near latitude 40° N (latitude position represents generally a location offshore of the New York/New Jersey coast) and approximately 3 meters (10 feet) near latitude 33.2° N (offshore of the South Carolina coast). The model simulated a maximum deepwater tsunami amplitude of about 3.5 meters (11.5 feet) near 28° N (offshore of Palm Bay, Florida) (Figure 8-3c of Reference 202). The relatively small tsunami amplitude near Units 6 & 7 is primarily a result of the presence of the Bahama

platform to the east, as shown in Figure 2.4.6-208. AGMTHAG did not model the propagation of tsunami waves across the continental shelf (water depth less than 250 meters or 820 feet) and run-up (Reference 202).

A similar tsunami model study was also performed by the West Coast and Alaska Tsunami Warning Center using a two-dimensional hydrodynamic model developed at the University of Alaska, Fairbanks (Reference 211). Four hypothetical worst-case scenarios with tsunami sources located in the Gulf of Mexico and the Caribbean regions were simulated using the West Coast and Alaska Tsunami Warning Center model. The simulations predicted the peak tsunami amplitude near Virginia Key, Florida, to be approximately 15 centimeters (0.5 foot) for an earthquake magnitude M_w of 9.0 in the Puerto Rico Trench. The simulated earthquake is larger in magnitude than any recorded earthquake in this region. The maximum recorded earthquake magnitude in this region is 8.3 (unknown earthquake scale) that struck the Guadeloupe Island in Lesser Antilles, as obtained from the National Geophysical Data Center (NGDC) earthquake database (Reference 212). Also tabulated in the NGDC earthquake database are two events with earthquake surface wave magnitude (M_s) of 8.1 that occurred near Haiti in 1842 and the Dominican Republic in 1946.

2.4.6.1.6 Other Sources

An extensive literature search did not return any information of seismically induced seiche in Biscayne Bay. In addition, because of low and flat topography near Units 6 & 7, the possibility of any subaerial slope failure that would generate tsunamis affecting Units 6 & 7 is precluded.

Earthquakes within the Gulf of Mexico are also recorded with epicenters located within the North American plate boundaries. Such “midplate” earthquakes are less common than earthquakes occurring on faults near plate boundaries and are unlikely to produce any destructive tsunami (Reference 213).

A significant tsunami generated directly by an earthquake only occurs if the earthquake is large (magnitude, with few exceptions, greater than about 6.5) and if the fault slip associated with the earthquake has a significant vertical seafloor displacement (thrust or normal faults). There is no record of surface fault rupture and significant seismic wave displacement at the seafloor associated with any historical earthquake in the central and eastern United States including the 1886 Charleston, South Carolina event of about magnitude 7, the largest historical earthquake in the U.S. Atlantic coastal region. Consequently, the conditions for tsunamigenesis by seafloor displacement associated with an earthquake do not

appear to exist along the U.S. Atlantic margin; Units 6 & 7, therefore, would not be impacted by significant tsunamis as a result of vertical seafloor displacement associated with the U.S. Atlantic margin earthquakes.

Although the north Caribbean subduction zone is noted for several seismically-generated tsunamis in recent times, as described in Subsection 2.4.6.1.5, potential submarine landslides of the carbonate platform edge north of Puerto Rico are capable of producing large tsunamis locally (see Subsections 2.4.6.2 and 2.5.1.1.5 for detailed discussions). However, because the Units 6 & 7 site is sheltered by the Bahamas Islands, such landslide-generated tsunamis are not expected to affect the site. Therefore, a landslide in the carbonate platform north of Puerto Rico is not considered as a PMT source for the Units 6 & 7 site.

2.4.6.1.7 Summary of Potential Sources for PMT at Units 6 & 7

Units 6 & 7 are not located in the immediate vicinity of any tsunamigenic source. The landslide zone nearest to Units 6 & 7 is located on the west Florida slopes within the Gulf of Mexico, separated by a very wide and shallow continental shelf and the entire width of the Florida peninsula. There is no historical evidence of any tsunami from landslides in the Gulf of Mexico. Landslides in the U.S. Atlantic margin may potentially generate local destructive tsunamis. However, because Units 6 & 7 are located far away from any such sources, is mostly sheltered by the Bahama platform, and is protected by a retaining wall structure with top elevation of 20.0 feet to 21.5 feet NAVD 88, such tsunamis are not expected to cause any flooding concern to the safety-related facilities of Units 6 & 7. The orientation of the Puerto Rico trench and the presence of the Bahama platform prevents any destructive tsunami to impact Units 6 & 7 from this source. Therefore, it is concluded that the PMT would likely be caused by earthquake-generated transoceanic tsunamis from the Azores-Gibraltar plate boundary. Characteristics of tsunami source generators for both Azores-Gibraltar plate boundary and Caribbean region are presented in Subsection 2.4.6.3.

2.4.6.2 Historical Tsunami Record

Records of historical tsunami run-up events along the U.S. Atlantic coast near Units 6 & 7 are obtained from the NGDC tsunami database (Reference 214). The NGDC database contains information on source events and run-up elevations for tsunamis worldwide from approximately 2000 B.C. to the present time (Reference 214). A search of the NGDC tsunami database returned 11 historical tsunamis that have affected the U.S. and Canada east coast, as indicated in Table 2.4.6-202.

Three events in the record are the result of a combination of earthquakes and submarine landslides in the Nova Scotia margin off the coast of Newfoundland, Canada, and in the Labrador Sea off Newfoundland, Canada. The most recent and most severe tsunami from this area was that from the M_w = 7.2 earthquake and associated submarine landslide in the Nova Scotia margin in 1929. The ensuing tsunami, with a maximum run-up of approximately 7 meters (23 feet) at Taylor's Bay, Newfoundland, Canada, was recorded as far south as Charleston, South Carolina (12 centimeters or 4.7 inches).

Three earthquakes in the Caribbean region generated tsunamis that were recorded in the U.S. east coast. The strongest earthquake was the M_s = 8.1 earthquake of August 4, 1946, with an epicenter northeast of the Dominican Republic, which was followed by the August 8, 1946 aftershock (magnitude 7.9 of unknown scale). The maximum tsunami run-ups from the two events were 5.0 meters (16.4 feet) and 0.6 meter (2.0 feet) at the coasts of Dominican Republic and Puerto Rico, respectively, for the August 4 and August 8 events. No run-up data is available from these events on the Florida Atlantic coast. The other tsunami event was caused by the earthquake of 1918 (M_w = 7.3) in Mona passage, located northwest of Puerto Rico, resulting from the displacement of four segments of a normal fault (Reference 214). A recent study hypothesized a combined earthquake- and landslide-generated tsunami for this event (Reference 215). The NGDC database indicates a tsunami amplitude of 6 centimeters (2.4 inches) near Atlantic City, New Jersey. However, no run-up was reported on the Florida Atlantic coast from this event. The maximum tsunami amplitude from this event reported along the western and northern Puerto Rico was 6.1 meters (20.0 feet).

The NGDC database also includes three tsunami events generated in the U.S. Atlantic margin with the Charleston, South Carolina, earthquake-generated (M_w = 7.7) tsunami of 1886 being the only confirmed tsunami. An earthquake event was also reported at Jacksonville, Florida, on the same day approximately an hour before the Charleston, South Carolina, earthquake. It has not been established if the two events were related (Reference 214). The resulting tsunami waves were reported in Jacksonville and Mayport, Florida, although no run-up information is available. The two other tsunami events are reported as probable in the NGDC database. The first tsunami event was the result of an earthquake in High Bridge, New Jersey (magnitude computed from the felt area, Mfa = 4.4) that produced a tsunami-like wave in Long Island, New York, in 1895. The second event was a possible landslide- or explosion-generated tsunami near Long Island, New York, that produced a maximum tsunami amplitude of 0.28 meter (0.9 foot) at

Plum Island, New York, in 1964. No tsunami wave from the two events was reported in the Florida Atlantic coast.

The remaining two records in the NGDC database are transoceanic tsunami events: the Great Lisbon Earthquake tsunami of 1755 off the Portugal coast and the Boxing Day tsunami of 2004 off the west Sumatra coast, Indonesia. The earthquake west of Sumatra (M_w = 9.0) generated a tsunami that was recorded nearly worldwide and killed more people than any other tsunami in recorded history (Reference 214). A tsunami amplitude of 0.17 meter (0.6 foot) was recorded at Trident Pier on the Florida Atlantic coast. The Great Lisbon Earthquake that destroyed the city of Lisbon stuck at approximately 9:40 a.m. on November 1, 1755. Mader reported an estimated magnitude (M_w) of approximately 8.75–9.0 for the earthquake that was felt over an area of a million square miles (Reference 209). The earthquake generated a tsunami, which arrived at Lisbon between 40 minutes and 1 hour after the earthquake as a withdrawing wave, that emptied the Lisbon Oeiras Bay (Reference 209). The following tsunami wave arrived with an amplitude of approximately 20 meters (65.6 feet) followed by two more waves approximately an hour apart (Reference 209). The tsunami wave had amplitudes of 4 meters (13.1 feet) along the English coast, and 7 meters (23 feet) at Saba, Netherland Antilles, in the Caribbean after approximately 7 hours of travel (Reference 209). Lockridge et al. also reported tsunami arrival in the harbor at Cape Bonavista, Newfoundland, Canada, with a retreating wave and a subsequent returning wave approximately 10 minutes later (Reference 208). Model simulation by Mader showed that the tsunami wave arrived at the Florida Atlantic coast approximately 8 hours after the earthquake (Reference 209). The deepwater tsunami amplitude off the coast of Miami, Florida, was simulated to be approximately 2 meters (6.6 feet) with a period between 1.25 and 1.5 hours. Mader suggested a maximum tsunami amplitude of approximately 3.0 meters (10 feet) including wave run-up along the U.S. east coast (Reference 209).

Lockridge et al. reported tsunamis and tsunami-like events in the U.S. east coast in addition to the events reported in the NGDC database (Reference 208). Most of these additional events originated along the New York, New Jersey, and Delaware coasts, and the Florida Atlantic coast remained unaffected. No seismically-induced paleotsunami deposits have been positively identified in available scientific literature within the 200-mile radius of the Turkey Point site, as described in Subsection 2.5.1.1.5. Distinguishing characteristics of tsunami versus storm deposits are also described in Subsection 2.5.1.1.5. Turkey Point site boring log

data interpretation and relevance to paleotsunami deposits is described in Subsection 2.5.1.2.2

2.4.6.3 Source Generator Characteristics

There is no tsunamigenic source present in the immediate vicinity of Units 6 & 7. The submarine landslide zones in the U.S. Atlantic margin and along the Gulf of Mexico coast are located far away from Units 6 & 7 and are separated by a wide and shallow continental slope and shelf, which would reduce the impact of any landslide-generated tsunamis at Units 6 & 7. The north Caribbean subduction zone and Azores-Gibraltar plate boundary are identified as the primary tsunamigenic earthquake sources that could affect the site. Model simulation results indicate that the shallow Bahama platform shields Units 6 & 7 from tsunamis generated in the northern Caribbean region (Reference 211). Therefore, the PMT for Units 6 & 7 would likely be transoceanic tsunamis from the Azores-Gibraltar region. The most recent major earthquake in the region occurred in 1969 (M_w = 7.8) and generated a small tsunami amplitude locally (Reference 202).

2.4.6.3.1 Azores-Gibraltar Plate Boundary

The Azores-Gibraltar plate boundary separates the African and Eurasian plates and extends from Azores in the west at the junction of North American, African, and Eurasian plates to east of Gibraltar strait, the area southwest of the Iberian Peninsula (see Figure 2.4.6-206). Based on literature on plate kinematic models and focal mechanisms, AGMTHAG indicated that the motion between the two plates is slow, changing along the boundary from divergent extension in the Azores to compression towards the east end that includes the Gorringe Bank and the Gibraltar Arc (Figure 2.4.6-206). The location of plate boundary in the east near Iberia is uncertain where a diffuse compression zone exists over a 200–330 kilometers (124–205 miles) width. The dominant active structures in the region are the Gorringe Bank Fault (GBF), the Marqués de Pombal Fault (MPF), the St. Vincente Fault (SVF), and the Horseshoe Fault (HSF) (Figure 2.4.6-206) (Reference 202).

The source location of the 1755 earthquake is still the subject of research in the scientific community. AGMTHAG summarizes the three major views on fault solution for the 1755 earthquake (Reference 202). First, in 1996, Johnson (also in 2007, Grandin et al.) suggested a northeast-southwest trending thrust fault, possibly outcropping at the base of the northwest flank of the Gorringe Bank (GBF). Second, Zitellini et al. in 2001 (also Grácia et al. in 2003) suggested active thrusting along the MPF as the source located approximately 80 kilometers

(50 miles) west of Cape Sao Vincente. Third, Gutscher et al. in 2002 and 2006 (also Thiebot and Gutscher in 2006) proposed a fault plane in the western Gulf of Cádiz (Gulf of Cádiz Fault, GCF), possibly as part of an African plate subduction beneath Gibraltar (Reference 202).

AGMTHAG used the same set of fault parameters as proposed by Johnson to investigate constraints on the 1755 Lisbon earthquake epicenter, and potential tsunami hazard to the U.S. East Coast from possible future earthquake sources located in the east Atlantic region (Reference 202). The parameters are (Reference 202):

Source depth at the top of the fault plane = 5 kilometers (3.1 miles)
Length = 200 kilometers (124 miles)
Width = 80 kilometers (50 miles)
Dip = 40 degrees
Strike = 60 degrees
Average slip = 13.1 meters (43 feet)

The strike orientation as proposed for MPF and GCF sources differs considerably from the description for the GBF source proposed by Johnston. AGMTHAG investigated the effects of the variation in the location of earthquake epicenter and strike orientation on near-field and far-field tsunami amplitudes. Based on a comparison of model simulation results with reported tsunami amplitudes, AGMTHAG concluded that the 1755 earthquake was likely generated by a northwest-southeast trending fault located in the center of the Horseshoe plain south of Gorringe Bank (Reference 202).

2.4.6.3.2 Hispaniola-Puerto Rico-Lesser Antilles Subduction Zone

The Hispaniola-Puerto Rico-Lesser Antilles subduction zone was formed as the North American plate was subducting southwesterly beneath the Caribbean plate (Figure 2.4.6-207) (Reference 202). Relative plate movement changed to a more easterly direction resulting in a more oblique subduction beginning at 49 million years ago, which remained fairly stable afterwards as evidenced by the opening of the Cayman Trough between Cuba and Honduras (Reference 202). AGMTHAG describes the present subduction at the Puerto Rico trench as an old oceanic crust of 90–110 million years in age, subducting under Puerto Rico and Virgin Islands and at the Hispaniola trench as a thick crust of an unknown origin, which underlies the Bahama platform (Reference 202).

Although there are geometric similarities between the Puerto Rico trench and Sumatra-Andaman trench where the devastating 2004 Indian Ocean tsunami originated, AGMTHAG pointed out that the slip during the earthquake in the Puerto Rico trench is highly oblique and nearly parallel to the convergence direction unlike the Sumatra-Andaman trench (Reference 202). This difference in the slip angles indicates the potential for only small deformations of the overlying Caribbean plate.

In contrast to the Puerto Rico trench, slip on the Hispaniola trench is sub-perpendicular to the trench. Therefore, a large vertical motion is expected for a given magnitude of slip. Unlike the Puerto Rico trench, where a normal thickness oceanic crust is subducting, the crust entering the Hispaniola trench is very thick and would likely allow more stress to accumulate resulting in large earthquakes to occur (Reference 202).

The rupture parameters for the Puerto Rico and Hispaniola trenches, as proposed by AGMTHAG, are listed below (Reference 202):

Puerto Rico Trench (single rupture)

Length = 675 kilometers along the trench between 68° W and 62° W
Depth = 5 to 40 kilometers (3.1 to 25 miles)
Dip = 20 degrees
Strike = 70 degrees
Slip = 10 meters (32.8 feet)
Slip direction = 60 degrees
Shear modulus = 3×10^{10} Pa (6.3×10^{8} pounds/square feet)
Earthquake magnitude, Mw = 8.85

Hispaniola Trench

Length = 525 kilometers (326 miles) along the trench between 73° W and 68° W
Depth = 0 to 40 kilometers (0 to 25 miles)
Dip = approximately 20 degrees
Strike = 95–102 degrees
Slip = 10 meters (32.8 feet) assuming complete rupture of the Hispaniola trench
Slip direction = 23 degrees
Earthquake magnitude, Mw = 8.81

The magnitude of the earthquake-generated tsunami is related to the slip vector. The direction of slip vector is given by the slip angle, or rake, which is measured in the plane of the fault from the strike direction to the slip vector showing the motion

of the hanging wall relative to the footwall. The slip (rake) angle of the fault is often estimated from analysis of focal mechanisms. In those cases where the slip angle cannot be directly measured, the assessment of the sense of slip could be based on an integration of direct observations of the fault and tectonic indicators (Reference 216). Based on dislocation theory, the amplitude of seafloor displacement is linearly proportional to the magnitude and direction of the slip vector, which vary for the dip-slip and strike-slip faults. The vertical displacement of an oblique-slip fault is estimated as the sum of the displacement fields derived from the dip-slip and strike-slip components.

AGMTHAG modeled three different source segments for the northern Puerto Rico/Lesser Antilles subduction zone, including the Puerto Rico and Hispaniola trenches (Reference 202). Tsunami propagation from these sources was modeled by linear long-wave theory, as described in AGMTHAG (Reference 202). The source parameters for the Puerto Rico and Hispaniola faults used in the model are slightly different than the source parameters described above and result in an earthquake moment magnitude ranging between 9.11 and 9.15. A summary of the tsunami source parameters including the expected range of magnitude and average slip angles for each tsunamigenic fault in Caribbean region is given in Table 8-1 of AGMTHAG (Reference 202).

2.4.6.4 Tsunami Analysis

The maximum tsunami water level at Units 6 & 7 is obtained for the postulated PMT generated by earthquake in the Azores-Gibraltar fracture zone. Tsunami propagation and the effects of near shore bathymetric variation at the Florida Atlantic coast are simulated in a two-dimensional computer model, the development of which is summarized in the following subsections. Detailed water level records near Units 6 & 7 are not available for tsunamis generated by past earthquakes in the Azores-Gibraltar fracture zone or in the Caribbean subduction zone for the listed earthquake magnitudes. In order to establish the model boundary condition, the resulting water levels in deep waters in the computer simulations by Mader (Reference 202) and Knight (Reference 211) for tsunamis generated from the Azores-Gibraltar and Caribbean sources are used as guidance for the PMT model. The PMT simulation for Units 6 & 7 uses the computer code Delft3D-Flow, which is a multi-dimensional modeling system that is capable of simulating the hydrodynamics and transport processes for fluvial, estuarine, and coastal environments (Reference 219).

2.4.6.4.1 Numerical Modeling Approach and Conceptualization

Subsection 2.4.6.1 establishes the Azores-Gibraltar fracture zone (specifically the 1755 Lisbon Earthquake source) as the candidate PMT source for Units 6 & 7. It is postulated that the earthquake-generated transoceanic tsunami from this source would propagate across the Atlantic Ocean and would be modified at the Bahama platform before reaching the site. Tsunami generation and transoceanic propagation from this source were studied previously using numerical model simulations (References 202 and 209). However, tsunami wave modification on the shallow Bahama platform and wave run-up onshore near Units 6 & 7 have not been reported in any literature. The primary objectives in developing the numerical model for Units 6 & 7 therefore are to account for the effects of near shore bathymetric variation on tsunami wave modification and tsunami run-up onshore.

Delft3D-FLOW, the flow module of the Delft3D modeling system, simulates two- or three-dimensional unsteady flow problems from tide or meteorological forcing. The FLOW module provides hydrodynamic solutions for which the horizontal length and time scales are significantly larger than the vertical scales (Reference 219) representing the shallow water conditions. Delft3D-FLOW has the capability of invoking the FLOOD solver, which employs a numerical technique (Reference 220) that can be applied to problems involving rapidly varied flows, for example, in hydraulic jumps and bores, and sudden flow transitions including rapid flooding and drying of land. The FLOOD scheme is suitable for simulating the tsunami waves, embankment breaches, hydraulic jumps, and flows over obstructions (Reference 219). Consequently, in the present analysis, the Delft3D-FLOW module along with the FLOOD solution scheme is applied to simulate tsunami propagation and run-up at Units 6 & 7.

Delft3D-FLOW assumes hydrostatic pressure distribution, ignores frequency dispersion, and does not include wave breaking mechanism. As a result, model simulation results on tsunami propagation generally show steeper wave fronts with larger wave amplitudes compared to analytical solutions or benchmark laboratory test results (Reference 221). The shallow water conditions adopted in Delft3D-FLOW therefore are capable of resolving the tsunami wave propagation where the frequency dispersion is not significant and would be conservative in simulating the near shore tsunami amplitude.

2.4.6.4.2 Model Setup

AGMTHAG and Mader reported modeling of the 1755 Lisbon Earthquake tsunami and included most of the Atlantic Ocean in the model domain (References 202 and 209). The PMT model for Units 6 & 7, on the other hand, a portion of the Atlantic Ocean and the Gulf of Mexico are considered in the model setup, as described below.

Model Domain and Grids

To be able to investigate nearshore tsunami wave modification and onshore run-up, the tsunami model domain is selected to include detailed bathymetric variations in the area bounded by the Atlantic continental shelf, the Florida platform, Cuba, Dominican Republic, and the Blake-Bahama basin (as shown in Figure 2.4.6-209). In light of the uncertainties in defining the 1755 Lisbon Earthquake source in the Azores-Gibraltar region (References 202 and 209), tsunami generation at the source was not included in the model. Instead, the model (open) boundary in the Atlantic Ocean is established based on tsunami propagation patterns reported in existing literature, as described in Subsection 2.4.6.4.3.

The selected model domain is shown on Figure 2.4.6-210. The east model boundary in deep waters generally follows the simulated propagation of tsunami wave front after 6.5 hours of travel in Mader's analysis (Reference 209). The 6.5 hour wave front is selected to maximize the coverage of the ocean in the model and also allow the model to be defined by one open sea boundary with a uniform boundary condition. This open boundary extends from Havelock, North Carolina to north east of the Dominican Republic. The north and west model boundaries follow mostly the coastlines of the southeastern United States. The south model boundary is set along the northern coastlines of the Dominican Republic, Haiti, and Cuba. The small passage between Haiti and Cuba is conservatively assumed to be blocked. Southwest of the site, the model includes a portion of the Straits of Florida, the area protruding past the Florida Keys, to allow the tsunami wave to travel farther into the Gulf of Mexico so that the effect of this boundary on the site is minimized. Extending the model farther into the Gulf of Mexico is not necessary, as the maximum tsunami water level at the site would occur before the effect of this boundary is reflected back at the site. Consequently, the model boundary in the Gulf of Mexico is simulated as a closed boundary.

The model uses curvilinear orthogonal grids that are generated with RGFGRID, the Delft3D module for grid generation and processing. The curvilinear option

allows fitting grids cells along coastlines and contours of changing bathymetry. In addition, curvilinear grids could be oriented in relation to anticipated flow direction or wave propagation, thereby improving model accuracy.

A nested grid system with three different grid resolutions is developed using the domain decomposition tool within RGFGRID to appropriately resolve tsunami wave modification near the site. The three grid subdomains are shown on Figure 2.4.6-210. The first subdomain, SITE, covers the area near the site including the Biscayne Bay and the adjacent Straits of Florida, and has the finest grid resolution. The second subdomain, ISLANDS, includes most of the Bahamas with intermediate grid resolution. The third subdomain, DEEP, covers the rest of the model domain with a coarse grid resolution, which is mostly deep waters and is farther away from SITE and ISLANDS subdomains. At the interfaces between the subdomains, every third point in the finer grid is aligned with successive grid points in the coarser grid. Subdomain grid resolutions, represented by the square root of grid cell area, and grid spacings in the two orthogonal directions are given in Table 2.4.6-203. Figures 2.4.6-211 through 2.4.6-213 show the grids of the three subdomains.

Model Bathymetry

Tsunami model bathymetric and topographic data are obtained from the following public sources:

- Biscayne Bay sounding data from NOAA estuarine bathymetric database
- LiDAR (Light Detection And Ranging) data from NOAA Coastal Ocean Service database
- Coastal Relief data from NOAA National Geophysical Data Center (NGDC)
- ETOPO1 data from NOAA NGDC

The last two sources include both bathymetric and topographic (land) data, whereas the first source includes only bathymetric data, and the second source includes only topographic data. The four data sets have different horizontal and vertical resolutions. The Biscayne Bay sounding and LiDAR data have high vertical and horizontal resolutions compared to the Coastal Relief and ETOPO1 data. Therefore, they were given high priority and used first in populating the model depth data. The Coastal Relief data has higher horizontal resolution

compared to the ETOPO1 data and therefore was given priority in populating the remaining model domain. A summary of resolution of available data is given in Table 2.4.6-204.

Bathymetric data from all sources are projected to the Azimuthal Equidistant map projection centered at Unit 6 & 7 for a uniform horizontal datum description. The Azimuthal Equidistant map projection is used to minimize distortion in both distance and direction from the site. All bathymetric and topographic elevations are converted relative to mean sea level (MSL) from their original source datum. Conversion relationships between MSL and various vertical datums are selected based on NOAA's Virginia Key, Florida station.

The bathymetric and topographic elevations for the tsunami model are developed by using the Delft3D-QUICKIN module. Elevations at the grid points are determined by interpolating from the source data surrounding the grid points. Model bathymetric elevations at grid points with seabed located below the MSL are specified as positive, whereas, all grid points on land are given negative bathymetric (topographic) values. The developed model bathymetric map is shown on Figure 2.4.6-214.

Bed Roughness Condition

Bed roughness conditions in the tsunami model are specified through Manning's *n* roughness coefficient. A constant Manning's roughness coefficient of 0.025 is used for the entire model domain, which represents natural channels in good condition (Reference 222).

Initial Condition

The antecedent water level including the 10 percent exceedance high spring tide, initial rise, and long-term sea level rise, as specified in Subsection 2.4.5.2.2.1, is used as the initial water level for the tsunami model. The initial water level in the tsunami model, after conversion to MSL, is 1.36 meters (4.46 feet) MSL.

Time Step and Simulation Time

The tsunami model is run with a time step of 0.2 minute (12 seconds). The model simulations are continued for a period of 9 hours, although the travel time from the open boundary to the site is about 2.5 hours and the maximum tsunami water level at the site is reached after about 4.5 hours from the start of simulation. Therefore, simulation period of 9 hours is sufficient to capture the maximum water

level at the site. The start and end time for model simulations are selected arbitrarily.

2.4.6.4.3 Selection and Validation of Open Boundary Condition

The model requires time history of incoming tsunami water level as the boundary condition along the eastern open boundary. However, no measured water level data from the 1755 Lisbon Earthquake tsunami is available at the model boundary location. Consequently, a synthetic time history of tsunami water level assuming a sinusoidal tsunami waveform is used to establish the model boundary condition.

Tsunami water level on the Atlantic coast near Miami, Florida, is obtained from the model simulation results performed by Mader for the 1755 Lisbon Earthquake tsunami (Reference 209). Because the source location and characteristics for the 1755 Lisbon Earthquake are not precisely known, Mader developed tsunami source parameters in such a way that the model reproduces tsunami amplitude and arrival time within reasonable accuracy at near- and far-field locations where these are known. Mader assumed the source location to be close to Gorringe Bank in the Azores-Gibraltar region, near the source location of the 1969 earthquake (1969 earthquake location is shown on Figure 2.4.6-206). To produce a tsunami amplitude of 20 meters (65.6 feet) with a 1-hour wave period that arrives at Lisbon, Portugal, 40 minutes after the earthquake, Mader considered fracture in a 300 kilometers (186.4 miles) arc-fault with a slip of 30 meters (98.4 feet). Although Mader did not provide information on the strike angle or location, the curved fault structure resembles closely to the composite fault zone assumed by Gutscher et al. in 2002, 2006 and discussed in AGMTHAG (Reference 202). In addition, the slip magnitude assumed by Mader is higher than that listed in Subsection 2.4.6.3.

AGMTHAG also performed numerical model simulations of the 1755 Lisbon Earthquake tsunami to evaluate the potential tsunami impact on the U.S. east coast. AGMTHAG first investigated the constraints on the earthquake epicenter from far field simulations. AGMTHAG modeled three different source segments for the northern Puerto Rico/Lesser Antilles subduction zone including the Hispaniola, Puerto Rico and Virgin Island faults. The earthquake moment magnitude from the selected source parameters ranges between 9.11 and 9.15. Using a linear long-wave model, AGMTHAG obtained a maximum tsunami amplitude near the site of no more than 0.1 meter (0.3 foot), as described in Subsection 2.4.6.1.5. AGMTHAG simulated tsunami propagation for 16 such potential source locations as shown in Figure 2.4.6-215. Based on model simulation results, AGMTHAG concluded that the variation in local seafloor

bathymetry significantly controls tsunami propagation across the Atlantic Ocean. The Gorringe Bank and the Madeira Tore Rise (see Figure 2.4.6-206 for locations) act as near source barriers protecting most of the U.S. east coast. For sources located east of Madeira Tore Rise and south of Gorringe Bank, Florida might be at risk if sufficient wave energy passes through the Bahamas (Reference 202). AGMTHAG did not simulate tsunami wave run-up in the near shore region and considered relative amplitude evaluation only (Reference 202). Because the simulated deepwater tsunami amplitude in the southeastern U.S. coast from AGMTHAG is smaller than the tsunami amplitude reported in Mader (References 202 and 209), the present analysis adopted tsunami amplitude from Mader in developing the boundary condition in the tsunami model.

Mader performed numerical modeling of the tsunami wave using the SWAN nonlinear shallow water wave code including the Coriolis and friction effects. The model domain extended from 20° N to 65° N and 100° W to 0° W with a 10-minute grid resolution. Model bathymetry information was generated from the 2-minute Mercator Global Marine Gravity topography of Sandwell and Smith of the Scripps Institute of Oceanography (Reference 209). A model time step of 10 seconds was used for the simulation. Mader obtained tsunami amplitude of 20 meters (65.6 feet) at 953 meters (3127 feet) water depth off Lisbon, Portugal, and 5 meters (16.4 feet) at 825 meters (2707 feet) water depth east of Saba, Netherlands Antilles in the Caribbean. Mader argued that with a run-up amplification of the wave, the maximum near-shore wave amplitude would be two to three times the deepwater tsunami amplitude. However, he also pointed out that some of the run-up effects were probably included in the simulation for water depths less than 1000 meters (3281 feet). This assumption would provide a maximum tsunami water level above 20 meters (65.6 feet) at Lisbon and above 7 meters (23 feet) at Saba, higher than the tsunami amplitudes reported by Lockridge et al. (Reference 208). Consequently, simulated water levels obtained by Mader along the U.S. east coast would likely be conservative. Mader obtained tsunami amplitude of 2 meters (6.6 feet) at 783 meters (2569 feet) water depth east of Miami, Florida with a tsunami period of 1.5 hours, and suggested a maximum tsunami wave amplitude, including run-up, of approximately 10 feet (3 meters) along the U.S. east coast (Reference 209).

The synthetic tsunami marigram at the model boundary is selected such that the maximum tsunami wave amplitude and drawdown off Miami, Florida at a water depth of 783 meters (2569 feet) are comparable or conservative compared to Mader's results for the same location. Mader estimated the maximum wave amplitude and drawdown of 2.0 meters (6.6 feet) and -3.5 meters (-11.5 feet),

respectively, from the initial water level at MSL (Reference 209). To generate the tsunami marigram at the model boundary, three different sinusoidal wave patterns are considered, each with 2.0 meter (6.6 feet) amplitude and 1.5 hours wave period. The first case considers a single wave, the second case considers a continuous wave train, and the third case considers only two consecutive waves. Figure 2.4.6-216 shows the marigrams for the three cases.

Figure 2.4.6-217 shows the simulated tsunami water levels for the three selected cases at the 783 meters (2569 feet) water depth off Miami, Florida. Similar to Mader, model simulations for the three cases consider the initial water level to be at MSL. Continuous wave train at the boundary generates the maximum tsunami amplitude and drawdown of about 5.5 meters (18 feet) and -6.5 meters (-21.3 feet), respectively, with respect to the MSL. These amplitude and drawdown are much higher than what is indicated in Mader's analysis, and therefore model input conditions with continuous wave train are not considered to be realistic. The single wave boundary condition produced the maximum wave amplitude and drawdown of about 2 meters (6.6 feet) and -3.5 meters (-11.5 feet), respectively, which are in very good agreement with Mader's results. However, because more than one wave was reported to have impacted the Portuguese and Canadian coasts (References 208 and 209), the single wave boundary condition is not considered in the present analysis. The boundary condition with two consecutive waves generates the maximum wave amplitude and drawdown of 4.5 meters (14.8 feet) and -5.3 meters (-17.4 feet), respectively. Although these values are much higher compared to Mader's results, they are conservatively adopted for this analysis. This tsunami amplitude is also much higher than the tsunami amplitudes reported in AGMTHAG for many different earthquake source locations and orientations in the Azores-Gibraltar fracture zone and for the Caribbean sources (Reference 202).

2.4.6.4.4 Sensitivity of Model Parameters

Model sensitivity analysis is conducted for the following parameters: grid size, time step, Manning's n value, tsunami wave period, and Coriolis effects.

Grid Size

Model grid configuration is selected based on bathymetric data resolution, computational economy, etc. A finer mesh model grid is developed as part of grid size sensitivity analysis to demonstrate that the selected grid sizes resolves the required flow problems reasonably well. In the finer mesh model, grid sizes for the ISLANDS and SITE subdomains are refined by a factor of 5/3 (1.67), whereas the

grid sizes in subdomain DEEP remained unchanged because of computational economy. Additionally, because the DEEP subdomain is located farther away from the site and in high water depths, a finer grid resolution in this area is not expected to produce any significant variation in tsunami water level at the site. The difference in tsunami water levels at the site from the two grid descriptions is very small, as shown in Figure 2.4.6-218. The selected coarser grid configuration therefore is considered adequate.

Time Step

Model simulations are performed with a computational time step of 0.2 minute (12 seconds). However, to demonstrate time step independence, a model simulation with 0.1 minute (6 seconds) time step is performed. Because the water levels at the site from the two simulations are nearly identical, the use of 12 seconds time step is considered acceptable.

Manning's *n* value

Model simulations are performed for two additional Manning's *n* values of 0.02 and 0.03. The results indicate that a lower Manning's *n* value produces a higher water level at the site. However, for this analysis a Manning's *n* of 0.025 is selected based on typical coastal area surface characteristics (Reference 222). Because the selected boundary condition provides conservative tsunami amplitude at the site, as described in Subsection 2.4.6.4.3, the selected bed roughness conditions are considered adequate.

Tsunami Wave Period

Mader indicated that for the 1755 Lisbon Earthquake tsunami, the eastern U.S. coast, and the Caribbean would experience tsunami wave periods varying between 1.25 and 1.5 hours (Reference 209). Results from an additional model simulation with a tsunami wave period of 1.25 hours show that the maximum water level at the site is lower than maximum water level from the selected wave period of 1.5 hours. Therefore, the selected wave period is adopted in this analysis.

Coriolis Effects

Coriolis forces depend on the latitude and angular velocity of earth's rotation on its own axis. Model simulation results with and without Coriolis forces indicate that the effect of Coriolis force on the maximum water level at the site is insignificant. Coriolis forces therefore are not considered in model simulations.

2.4.6.4.5 Model Simulation Results

As described in Subsections 2.4.6.4.2 and 2.4.6.4.3, the maximum tsunami water level at the site is simulated for a boundary condition with two consecutive sinusoidal tsunami waves of 2.0 meters (6.6 feet) amplitude and 1.5 hours wave period. This boundary condition approximates the 1755 Lisbon tsunami that was generated at the Azores-Gilbaltar region, as simulated by Mader (Reference 209). An initial water surface elevation of 1.36 meters (4.46 feet) MSL is used to evaluate the maximum tsunami water level at the site.

Water level contours at different times are plotted to track the tsunami wave propagation from the open boundary to the site. These time-lapsed snap-shots of water level contours are given in Figures 2.4.6-219a through 2.4.6-219i. As the figures indicate, the tsunami waves propagate from the open boundary to Blake-Bahama Escarpment unimpeded and nearly perpendicular to the escarpment. As the waves reach the Bahama platform, tsunami waves north of the platform (north of Grand Bahama and Abaco Islands) are diffracted southwestward towards the Straits of Florida. The diffracted waves propagate through the Straits of Florida before reaching the site. The tsunami waves reaching the platform are affected by shoaling and travel through the channels and passages between the islands of the Bahamas. These transmitted tsunami waves then interact with the diffracted waves from the north.

From the Straits of Florida the tsunami waves enter the Biscayne Bay first through the openings, cuts, and channels in the barrier islands, and then by overtopping the barrier islands before affecting the site. The maximum tsunami water level at the site is reached as the barrier islands are overtopped. Water level contours in Biscayne Bay corresponding to the time close to the maximum water level at the site is shown in Figure 2.4.6-220.

The site is protected by the Bahamas from direct impact of the tsunami waves. The diffracted tsunami waves have less energy and therefore less flooding potential at the site. In addition, the islands and the vast extent of the Bahamas dissipate some of the tsunami wave energy before it reaches the deep waters of the Straits of Florida and ultimately the site.

Time history of tsunami water levels at key locations are plotted to show tsunami wave modification as it propagates and reaches shore. Figures 2.4.6-221a through 2.4.6-221d show the locations of the water level monitoring points. Track 1 (Figure 2.4.6-221a) generally follows tsunami wave propagation from the open boundary to east of the Bahamas and then the diffraction towards the Straits of

Florida. The tsunami marigrams for the monitoring points are given in Figure 2.4.6-222. The figure shows that as the tsunami waves travel from the open boundary towards the Bahamas, its amplitude increases due to shoaling. The maximum shoaling is seen near the edge of the escarpment north of Little Bahama Bank at monitoring point 4. Waves then dissipate on the shallow waters and diffract towards the Straits of Florida (points 5 and 6). The tsunami amplitudes increase as the diffracted waves interact with the waves passing through the Islands of the Bahamas (points 6 and 7). However, as the tsunami waves travel further south towards the site, its amplitude decreases slightly due to propagation and possibly friction loss.

For Track 2 (Figures 2.4.6-221b and 2.4.6-223), tsunami amplitudes increase as the waves shoal east of the Bahamas similar to that observed for Track 1. Between monitoring points 3 and 4, tsunami amplitude decreases slightly. At monitoring point 5 south of Grand Bahama Island, where the depth is relatively shallow, the wave amplitude increases due to shoaling. In the Straits of Florida, wave modifications are the same as described for Track 1.

Track 3 (Figures 2.4.6-221c and 2.4.6-224 shows modifications of tsunami wave amplitudes along the eastern U.S. Atlantic coast. Between monitoring points 1, 2, and 3, tsunami amplitudes remain nearly the same while the arrival time changes due to their distance from the boundary. However, tsunami amplitudes at monitoring points 4 through 7 are higher owing to the interaction of diffracted and propagated waves from the Bahamas.

Figure 2.4.6-225 shows tsunami marigrams in Biscayne Bay and vicinity. Grid cells (339, 270) and (339, 232) are located within the Straits of Florida adjacent to the site; grid cell (339, 172) is located between Biscayne Bay and the Straits at a shallow water depth (6.1 meters); and grid cells (339, 132), (339, 119), (307, 125), and (272, 146) are located within Biscayne Bay (Figure 2.4.6-221d). As shown in the figure, tsunami amplitudes within the Straits at the selected locations including the location with shallow water depth remain nearly the same. Water level variations within the Biscayne Bay, however, are markedly different compared to that in the Straits of Florida with the minimum water level in the bay considerably higher. This is because the barrier islands do not allow quick draining of the bay during tsunami drawdowns. In addition, the barrier islands dissipate wave energy during overtopping resulting in smaller wave amplitude and delayed arrival.

2.4.6.5 Tsunami Water Level

The time history of tsunami water level at the site is given in Figure 2.4.6-226. The maximum tsunami water level at the site from model simulation results is 4.17 meters (13.7 feet) MSL or 12.8 feet (3.9 meters) NAVD 88 including the initial water level of 1.36 meters (4.46 feet) MSL, which is rounded up to 14.0 feet (4.3 meters) NAVD 88. This maximum tsunami water level is 12 feet lower than the entrance floor elevation of all safety-related structures at 26 feet NAVD 88.

2.4.6.6 Hydrography and Harbor or Breakwater Influences on Tsunami

Units 6 & 7 are located adjacent to Biscayne Bay approximately 8 miles west of the Elliott Key barrier island. The PMT water level near Units 6 & 7 is analyzed based on published numerical simulation results and includes a conservatively assumed tsunami run-up. Therefore, the effect of hydrography of the area has been considered in the estimation of the PMT water level. There are no breakwaters located near the Units 6 & 7 that may affect the PMT water level.

2.4.6.7 Effects on Safety-Related Facilities

A conservative estimate of the PMT still water level near Units 6 & 7 is approximately 16.7 feet NAVD 88. This PMT water level along with coincidental wind-wave run-up, as presented in Subsection 2.4.5, would be lower than the design plant grade elevation of 26 feet NAVD 88 for the safety-related facilities. Therefore, the postulated PMT event does not affect the safety functions of Units 6 & 7. Because the PMT water level is lower than the design plant grade, debris, waterborne projectiles, sediment erosion, and deposits are not a concern to the functioning of the safety-related SSCs of Units 6 & 7.

2.4.6.8 References

201. Prasad, R., *Tsunami Hazard Assessment at Nuclear Power Plant Sites in the United States of America (Draft Report for Comments)*, Pacific Northwest National Laboratory, PNNL-1-7397, Office of New Reactors, NRC, NUREG/CR-6966, August 2008.

202. Atlantic and Gulf of Mexico Tsunami Hazard Assessment Group, *Evaluation of Tsunami Sources with the Potential to Impact the U.S. Atlantic and Gulf Coasts — An Updated Report to the Nuclear Regulatory Commission*, U.S. Geological Survey, Administrative Report, August 2008.

203. Twichell, D.C., Dillon, W.P., Paull, C.K., and N.H. Kenyon, *Morphology of Carbonate Escarpments as an Indicator of Erosional Processes, Geology of the Unites States Seafloor — A View from GLORIA*, Cambridge University Press, 1996.

204. Ward, S. N. and S. Day, "Cumbre Vieja Volcano — Potential Collapse and Tsunami at La Palma, Canary Islands," *Geophysical Research Letters*, Volume 28, No. 17, pages 3397–3400, 2001.

205. Mader, C.M., "Modeling the La Palma Landslide Tsunami," *Science of Tsunami Hazards*, Volume 19, No. 50–70, 2001.

206. Pararas-Carayannis, G., "Evaluation of the Threat of Mega Tsunami Generation from Postulated Massive Slope Failures of Island Stratovolcanos on La Palma, Canary Islands, and on the Island of Hawaii," *Science of Tsunami Hazards*, Volume 20, No. 5, pp. 251–277, 2002.

207. Gisler, G., Weaver, R., and M. L. Gittings, "Sage Calculations of the Tsunami Threat from La Palma," *Science of Tsunami Hazards*, Volume 24, No. 4, pp. 288-301, 2006.

208. Lockridge, P. A., Lowell, S. W., and J. F. Lander, "Tsunamis and Tsunami-Like Waves of the Eastern United States," *Science of Tsunami Hazards*, Volume 20, No. 3, pp. 120–157, 2002.

209. Mader, C.M., "Modeling the 1755 Lisbon Tsunami," *Science of Tsunami Hazards*, Volume 19, No. 2, pp. 93–98, 2001.

210. Lander, J.F., Whiteside, L.S., and P.A. Lockridge, "A Brief History of Tsunamis in the Caribbean Sea," *Science of Tsunami Hazards*, Volume 20, No. 2, pp. 57–94, 2002.

211. Knight, B., "Model Prediction of Gulf and Southern Atlantic Coast Tsunami Impacts from a Distribution of Sources," *Science of Tsunami Hazards*, Volume 24, No. 5, pp.s 304–312, 2006.

212. National Geophysical Data Center (NGDC), *Significant Earthquake Database*, revised August 27, 2008. Available at http://www.ngdc.noaa.gov/hazard/earthqk.shtml, accessed August 27, 2008.

213. National Earthquake Information Center, *M 5.8 Gulf of Mexico Earthquake of 10 September 2006*, U.S. Geological Survey, September 2006.

214. National Geophysical Data Center (NGDC), *Historical Tsunami Database*, revised August 27, 2008. Available at http://www.ngdc.noaa.gov/seg/hazard/tsu_db.shtml, accessed August 1, 2008.

215. Hornbach, M. J., Mondziel, S. A., Grindlay, N. R., Frohlich, C., and P. Mann, "Did a Submarine Slide Trigger the 1918 Puerto Rico Tsunami?," Science of Tsunami Hazards, Volume 27, No. 2, pp. 22–31, 2008.

216. Geist, E. L., *Local tsunamis and earthquake source parameters*, In: Tsunamigenic Earthquakes and their Consequences (Eds. R. Dmowska, and B. Saltsman) Advances in Geophysics, Volume 39, pp. 117–209, 1998.

217. ODP Shipboard Scientific Party, "Chapter 5. Site 626: Straits of Florida," *Proceedings Ocean Drilling Program*, Initial Report 101, p. 49-109, Austin, J. A. Jr., and Schlager, W. P., eds., 1986.

218. Iturralde-Vinent, M.A. (Ed.), *Geologia de Cuba para Todos, Edicion Cientifica, Museo Nacional de Historia Natural-CITMA*, preprint, 114 pages, 2009.

219. Deltares, Delft3D-FLOW, *Simulation of Multi-Dimensional Hydrodynamic Flows and Transport Phenomena, Including Sediments*, Rotterdamseweg 185, 2009.

220. Stelling, G.S. and Duinmeijer, S.P.A., "A Staggered Conservative Scheme for every Froude Number in Rapidly Varied Shallow Water Flows," *International Journal for Numerical Methods in Fluids*, v. 43, pp. 1329-1354, 2003.

221. Apotsos, A., Buckley, M., and Gelfenbaum, G., "Tsunami Benchmark Simulations Using Delft3D," *ISEC Community Workshop: Simulation & Large-Scale Testing of Nearshore Wave Dynamics, July 8-10, 2009 - Corvallis, Oregon*, 2009.

222. Imamura, F., Yalciner, A. C., and Ozyurt, G., *Tsunami Modeling Manual*, International Oceanographic Commission, 2006.

Table 2.4.6-201
Characteristics of Landslides on the U.S. Atlantic Margin

Dimension	Minimum	Maximum	Mean	Median
Area (square kilometer)	9	15,241	1,880	424
Length (kilometer)	2.7	>291	85	51
Width (kilometer)	2.1	151	21	12
Source Depth (meter)	92	3,263	1,630	1,785
Toe Depth (meter)	2,126	4,735	3,101	2,991
Scarp Height (meter)	3	410	90	63

Source: Reference 202

Table 2.4.6-202 (Sheet 1 of 2)
Summary of Historical Tsunami Run-Up Events in the East Coast of U.S.

Date[a]	Time (Hours)	Validity Code[b]	Cause Code[c]	Source Location (latitude, longitude)	Run-Up Location Along U.S. East Coast (lat, long)	Run-Up Type[d]	Run-Up Height (meters)
11/01/1755	08:50	4	1	Lisbon, Portugal (36.0°N 11.0°W)	—[e]	—	—
09/24/1848		3	8	Fishing Ships Harbor, Newfoundland, Canada (52.616°N 55.766°W)	—	—	—
06/27/1864	22:30	3	1	SW Avalon Peninsula, Newfoundland, Canada (46.5°N 53.7°W)	—	—	—
09/01/1886	02:51	4	1	Charleston, SC (32.9°N 80.0°W)	Jacksonville, FL (30.317°N 81.65°W) Mayport, FL (30.39°N 81.43°W) Copper River, SC (32.87°N 79.93°W)	1 1 1	—
09/01/1895	11:09	3	1	High Bridge, NJ (40.667°N 74.883°W)	Long Island, NY (40.591°N 73.796°W)	1	—
10/11/1918	14:14	4	1	Puerto Rico, Mona Passage (18.5°N 67.5°W)	Atlantic City, NJ (39.364°N 74.423°W)	2	0.06
11/18/1929	20:32	4	3	Grand Banks[f], Newfoundland, Canada (44.69°N 56.0°W)	Ocean City, MD (38.333°N 75.083°W) Atlantic City, NJ (39.35°N 74.417°W) Charleston, SC (32.75°N 79.916°W)	2 2 2	0.30 0.68 0.12
08/04/1946	17:51	4	1	Northeastern Cost, Dominican Republic (19.3°N 68.9°W)	Daytona Beach, FL (29.20°N 81.017°W) Atlantic City, NJ (39.364°N 74.423°W)	2 2	—
08/08/1946	13:28	4	1	Northeastern Cost, Dominican Republic (19.71°N 69.51°W)	Daytona Beach, FL (29.21°N 81.02°W) Atlantic City, NJ (39.364°N 74.423°W)	2 2	—
05/19/1964	00:00	3	8	Long Island, NY[f] (40.8°N 73.10°W)	Montauk, NY (41.033°N 71.950°W) Plum Island, NY (41.181°N 72.194°W) Willetts Point, NY (40.683°N 73.283°W) Newport, RI (41.493°N 71.327°W)	2 2 2 2	0.10 0.28 0.10 0.10
12/26/2004	00:58	4	1	Off Sumatra, Indonesia (3.295°N 95.982°E)	Trident Pier, FL (28.415°N 80.593°W) Atlantic City, NJ (39.35°N 74.417°W) Cape May, NJ (38.97°N 74.96°W)	2 2 2	0.17 0.11 0.06

Table 2.4.6-202 (Sheet 2 of 2)
Summary of Historical Tsunami Run-Up Events in the East Coast of U.S.

(a) Date and time given in Universal Coordinated Time (also known as Greenwich Mean Time).
(b) Tsunami event validity:
Valid values: 0 to 4
Validity of the actual tsunami occurrence is indicated by a numerical rating of the reports of that event:
0 = Erroneous entry
1 = Very doubtful tsunami
2 = Questionable tsunami
3 = Probable tsunami
4 = Definite tsunami
(c) Tsunami cause code:
Valid values: 0 to 11
The source of the tsunami:
0 = Unknown cause
1 = Earthquake
2 = Questionable earthquake
3 = Earthquake and landslide
4 = Volcano and earthquake
5 = Volcano, earthquake, and landslide
6 = Volcano
7 = Volcano and landslide
8 = Landslide
9 = Meteorological
10 = Explosion
11 = Astronomical tide
(d) Type of run-up measurement:
Valid values: 1 to 7
1 = Water height measurement
2 = Tide-gage measurement
3 = Deep ocean gage
4 = Paleodeposit
5 = Computer modeled
6 = Atmospheric pressure wave
7 = Seiche
(e) Data not available
(f) Only locations with measured run-up values are presented

Source: Reference 214

Table 2.4.6-203
Grid Resolution and Sizes of the Subdomains

	Grid Resolution (m)	Grid Spacing along M[(a)]Axis (m)	Grid Spacing along N[(a)] Axis (m)
SITE	450 - 540	260 – 410	620 – 800
ISLANDS	1,240 – 3,710	970 – 3,010	950 – 7,050
DEEP	3,120 – 22,320	1,850 – 24,080	2,630 – 27,340

(a) M and N are the principal axes of the model curvilinear grid system

Table 2.4.6-204
Horizontal and Vertical Resolutions of Depth Data

	Biscayne Bay Sounding	LiDAR	Coastal Relief	ETOPO1
Horizontal Resolution	30 m	0.1 m[(a)]	3 arc-seconds (90 m)	1 arc-minute (1,800 m)
Vertical Resolution	0.01 m	0.01 m	1 m for land 0.1 m for sea	1 m

(a) ~ 1 meter resolution for about 10 percent of the data

Figure 2.4.6-201 Location Map Showing the Extent of the AGMTHAG Study Area and Geologic Features That May Influence Landslide Distribution Along the U.S. Atlantic Margin

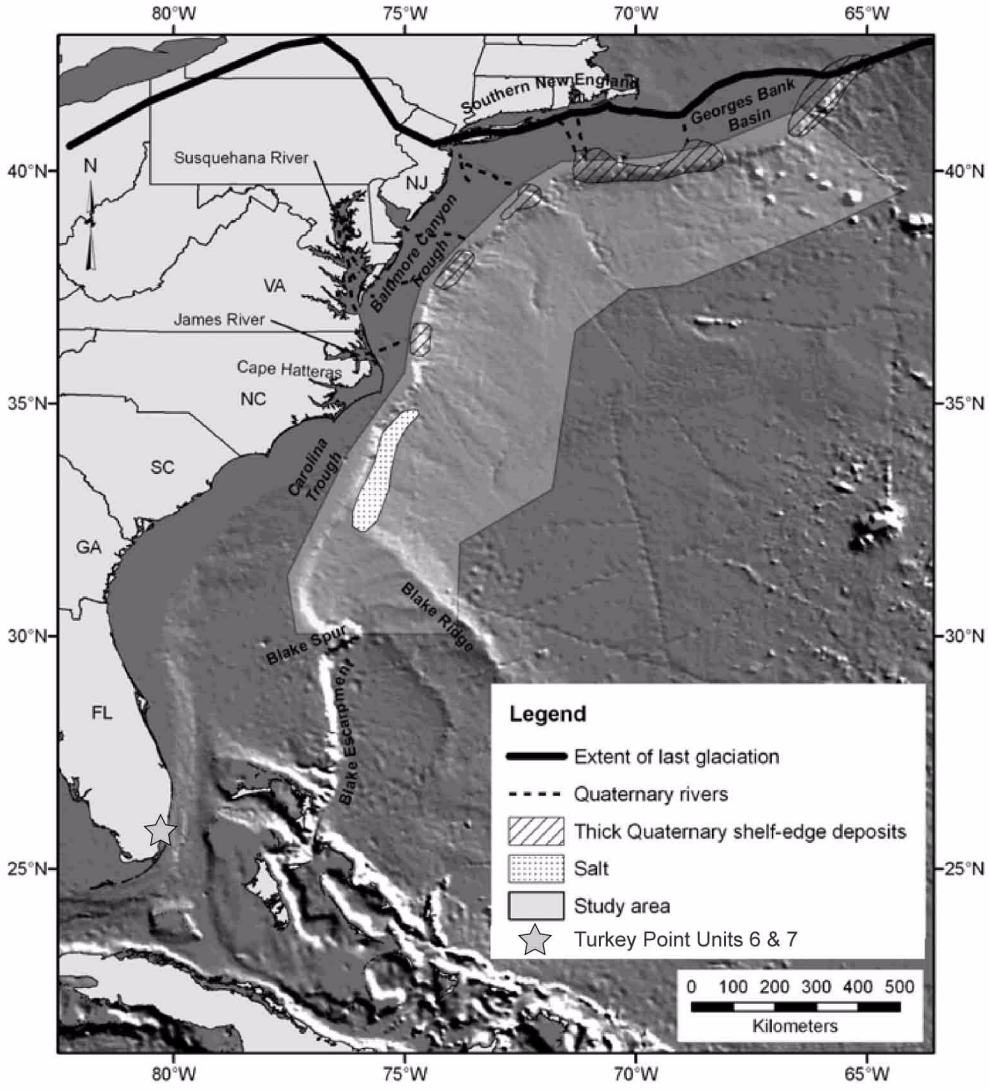

Modified from Reference 202

Figure 2.4.6-202 Distribution of Different Landslide Types Along the U.S. Atlantic Margin

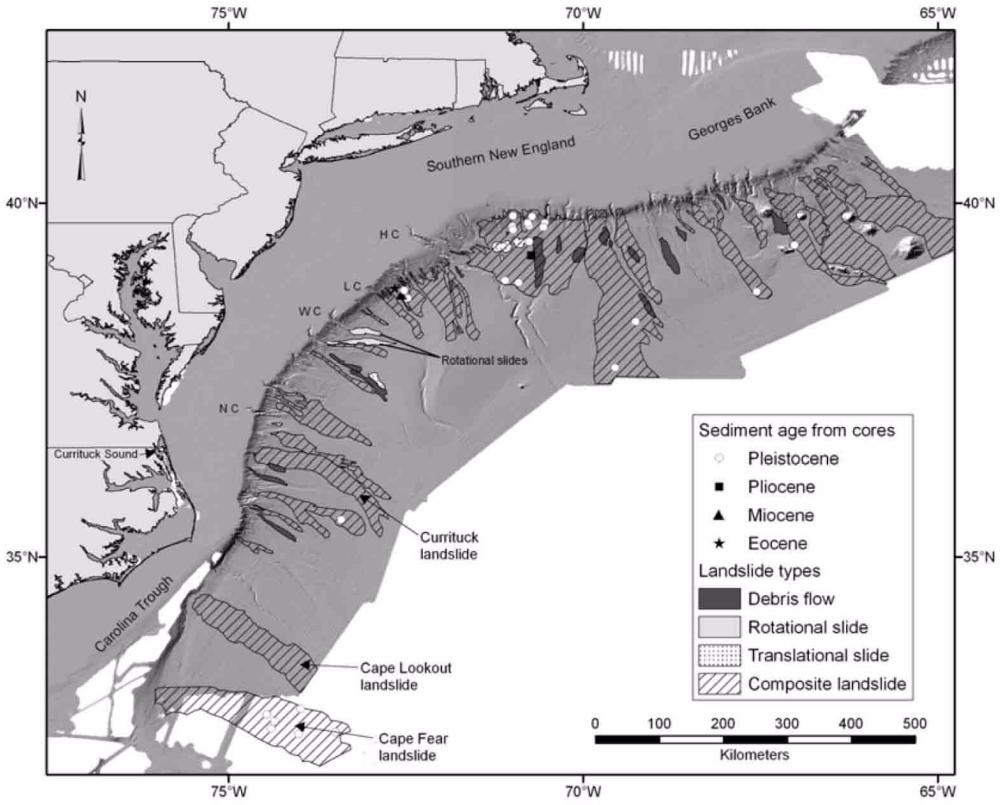

Notes: HC = Hudson Canyon; LC = Lindenkohl Canyon; WC = Wilmington Canyon; NC = Norfolk Canyon
Source: Reference 202

Figure 2.4.6-203 Location of Blake Escarpment Offshore of the Florida Coast

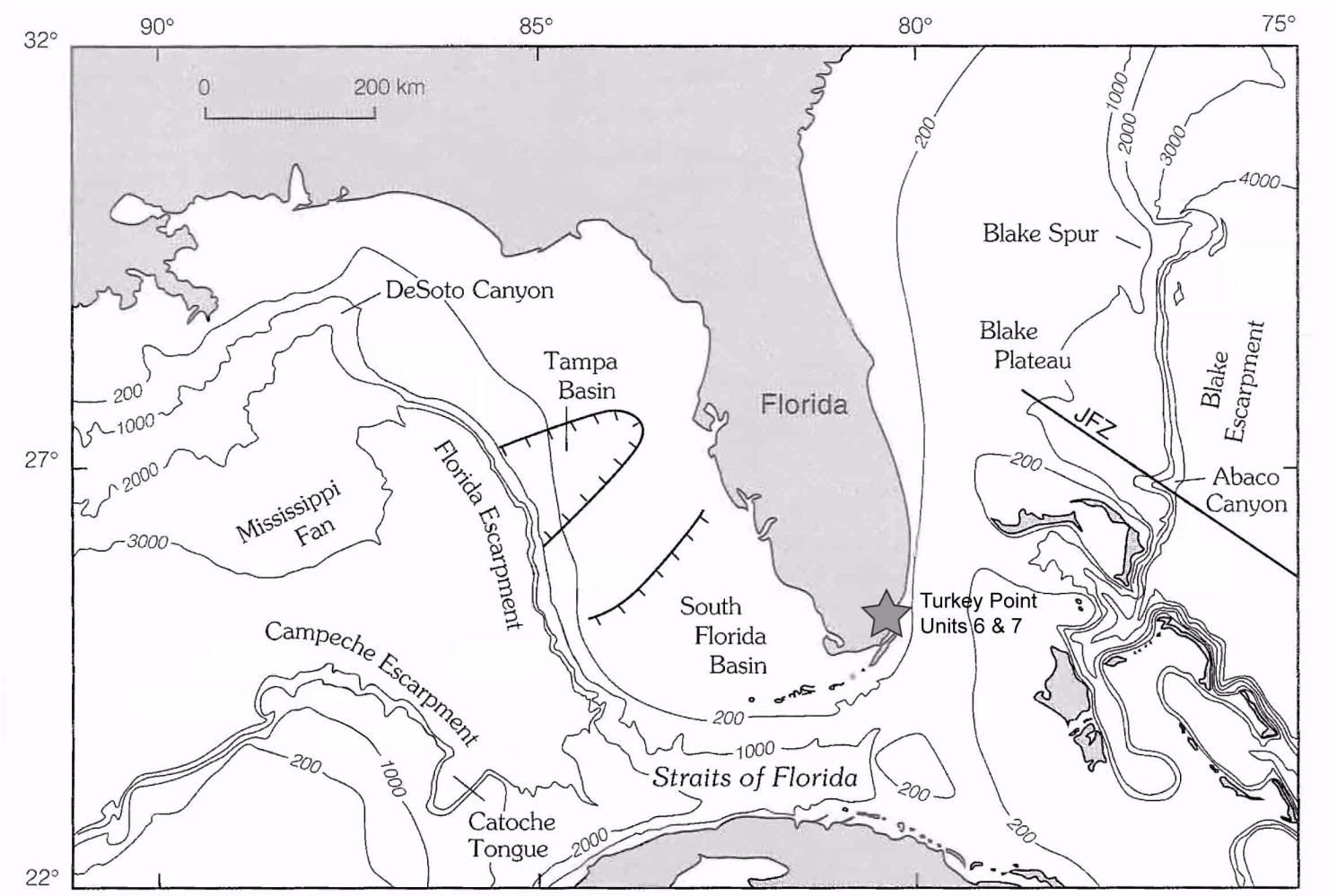

JFZ = Jacksonville fracture zone from Klitgord and Schouten (1986)

Note: Depth contours are in meters.
Modified from Reference 203

Figure 2.4.6-204 Location Map Showing the Extent of the Physiographic Features in the Gulf of Mexico Basin

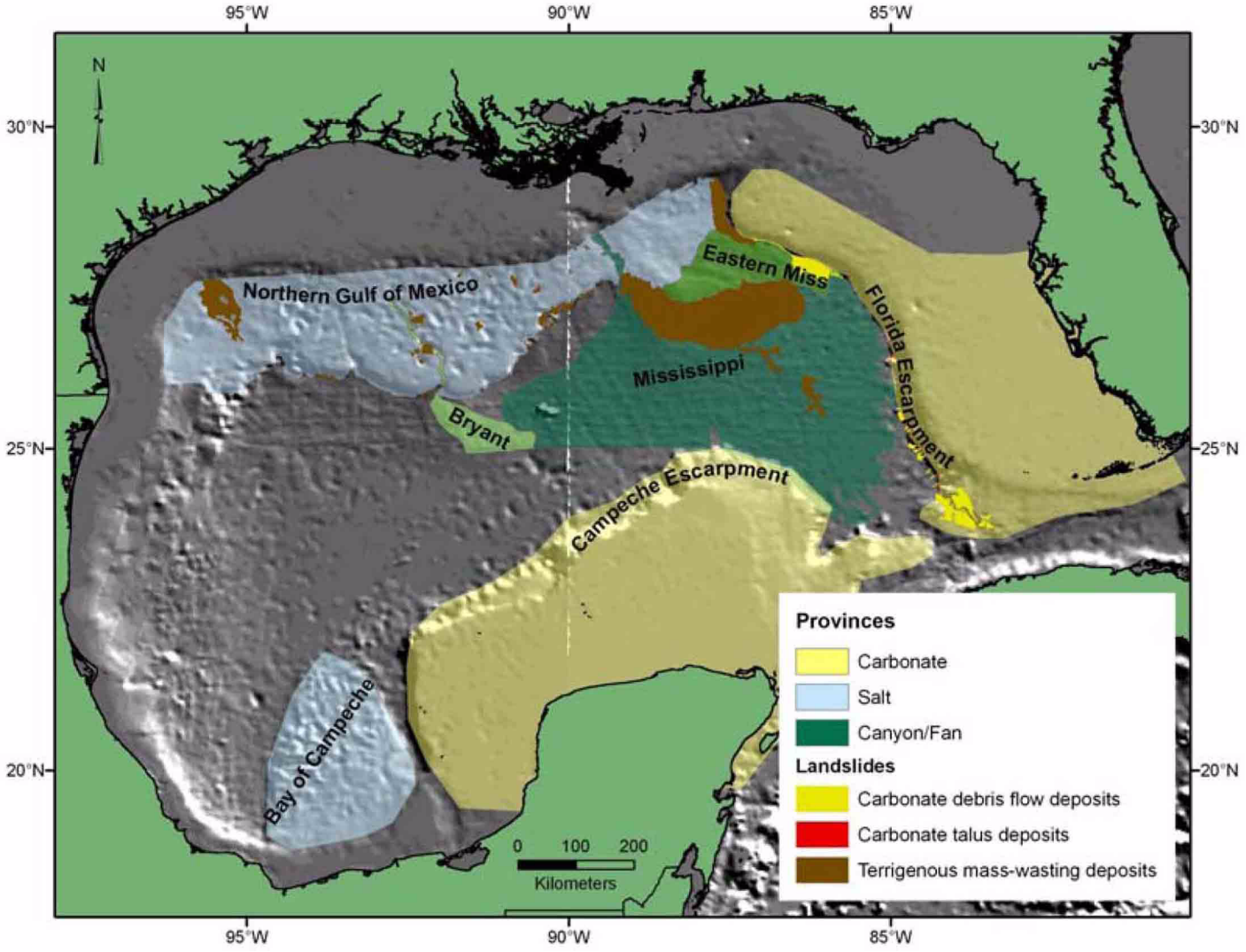

Source: Reference 202

Figure 2.4.6-205 (A) Morphology of the Florida Escarpment and the West Florida Slope, and (B) the Extent and Distribution of Carbonate Debris Flow Deposits and Talus Deposits

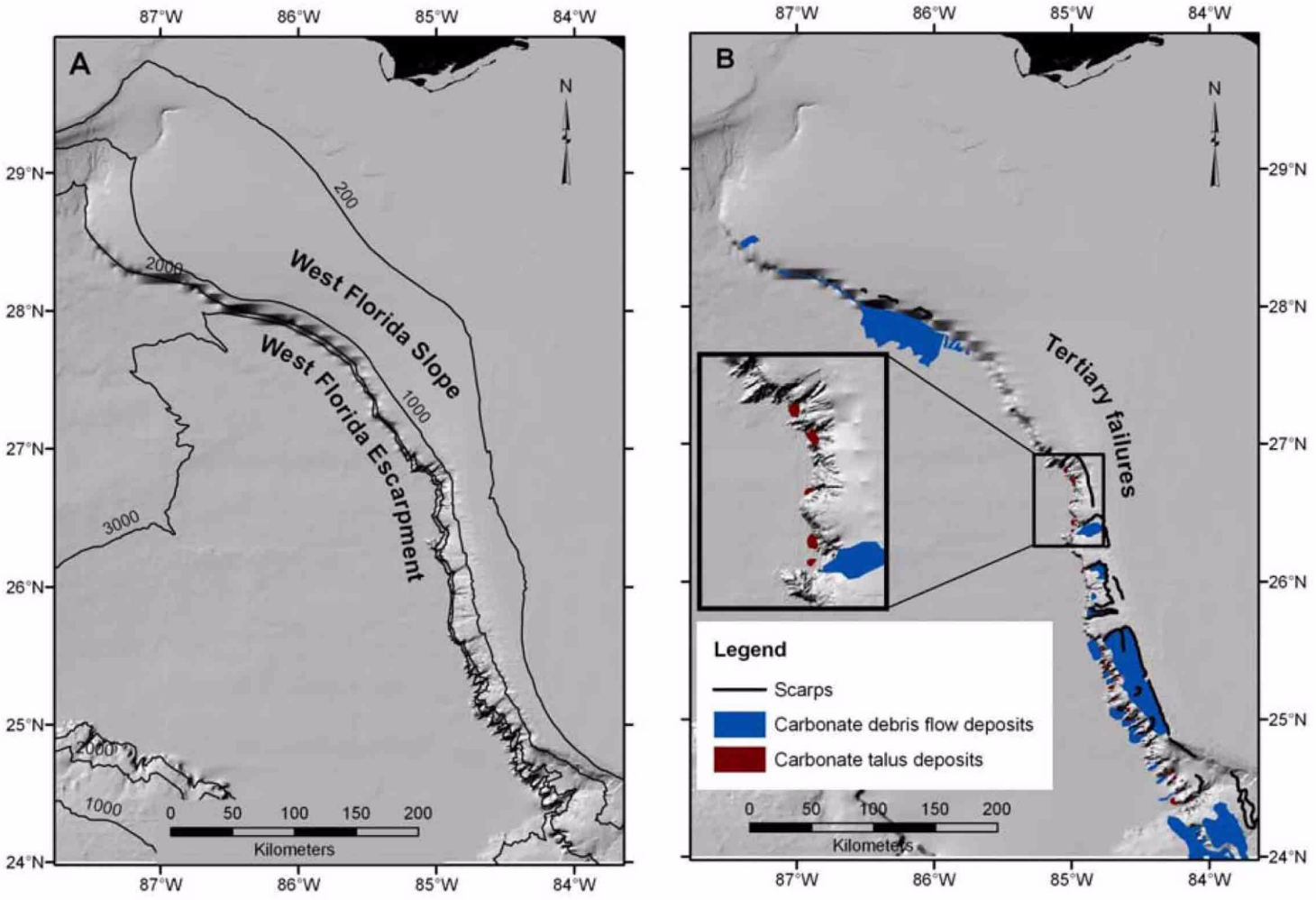

Note: Depth contours are in meters.
Modified from Reference 202

Figure 2.4.6-206 Plate Tectonic Setting and Bathymetry of the Eastern Azores-Gibraltar Region

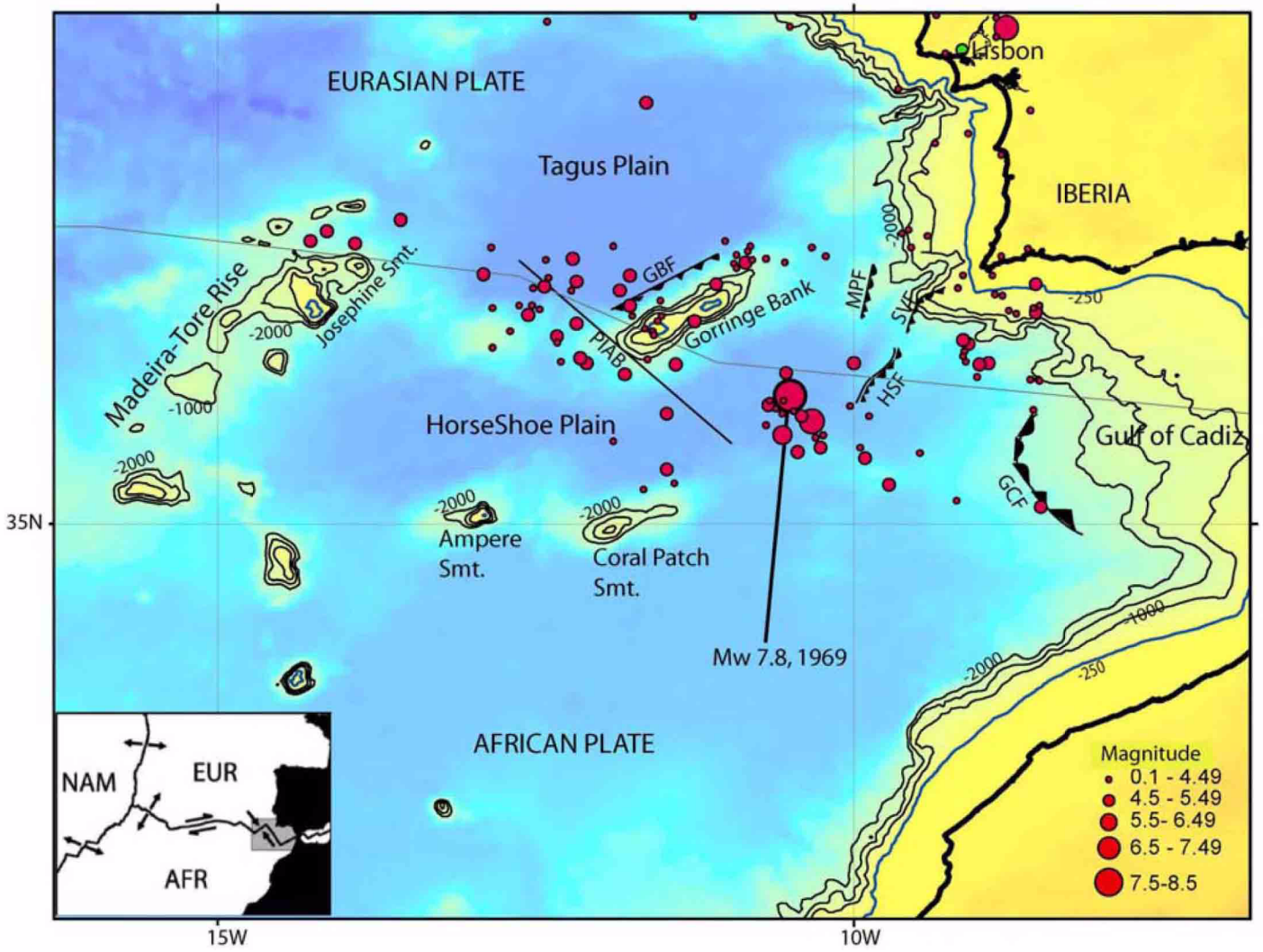

Note: Barbed lines show faults proposed in various past studies, GBF — Gorringe Bank Fault; MPF —- Marqués de Pombal Fault; SVF — St. Vicente Fault; HSF — Horseshoe Fault; GCF — Gulf of Cádiz Fault; PIAB - Paleo Iberia-Africa Plate Boundary. Inset plates: NAM - North American Plate; EUR — Eurasian Plate; AFR — African Plate. Depth contours are in meters (only contours from –250 to –2000 meters are shown).
Source: Reference 202

Figure 2.4.6-207 The Caribbean Plate Boundary and its Tectonic Elements

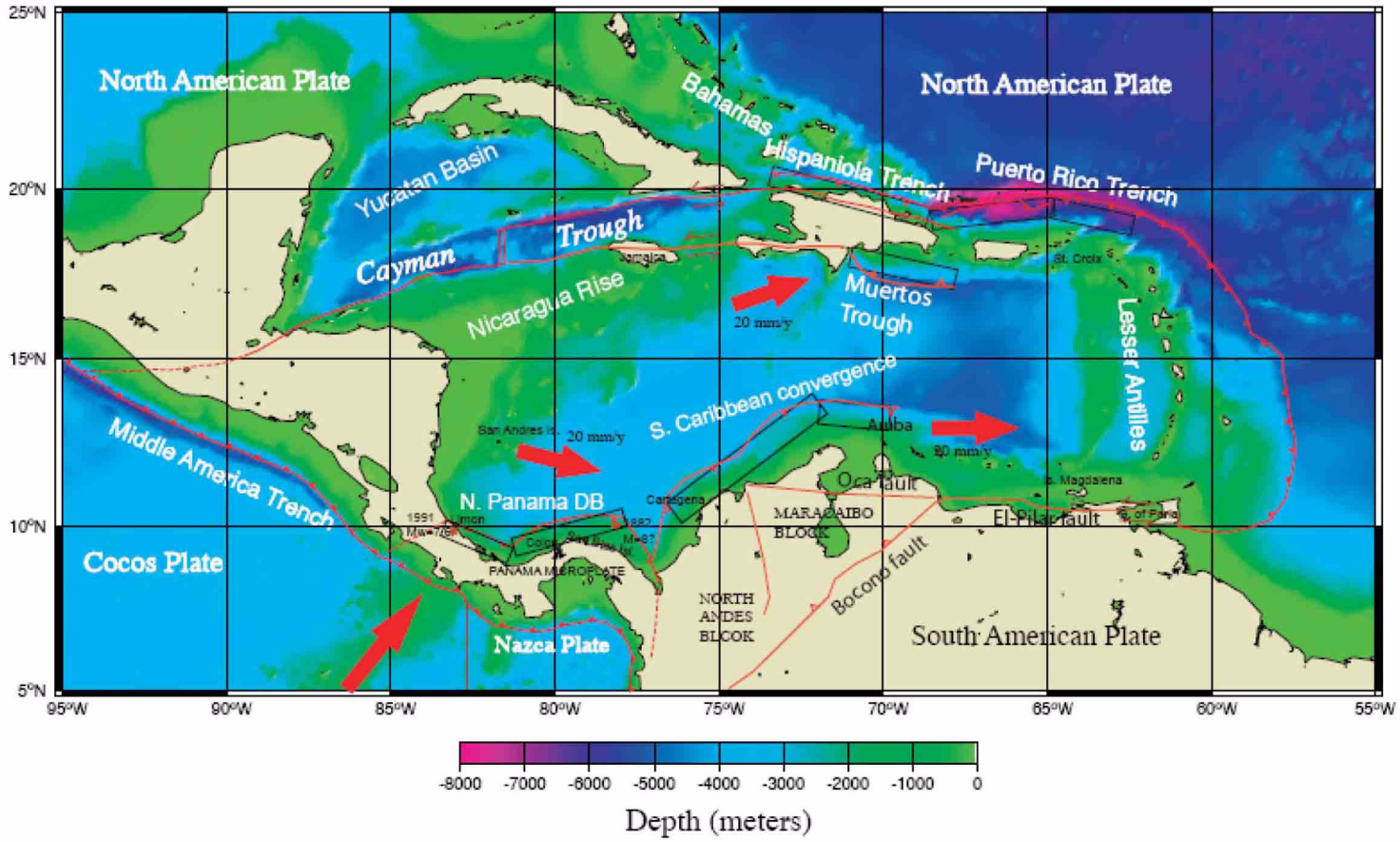

Note: Red lines are plate boundaries and red arrows indicate relative plate movement
Source: Reference 202

Figure 2.4.6-208 Perspective (Schematic) View of the Tectonic Elements in the Caribbean Plate and Seafloor Topography

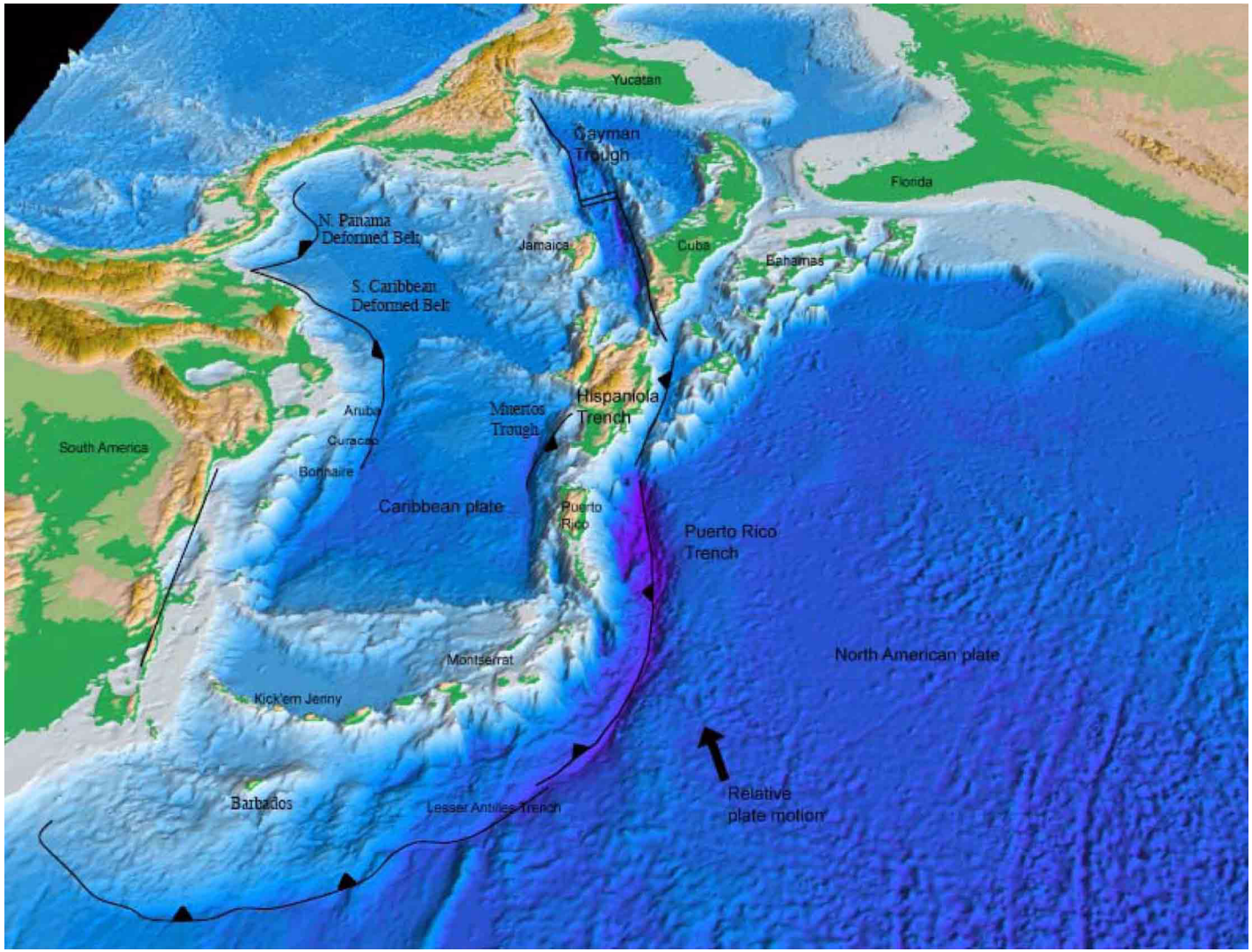

Source: Reference 202

Figure 2.4.6-209 Geophysical Setting and Seafloor Topography East of Southeast U.S. Coast and North of the Caribbean

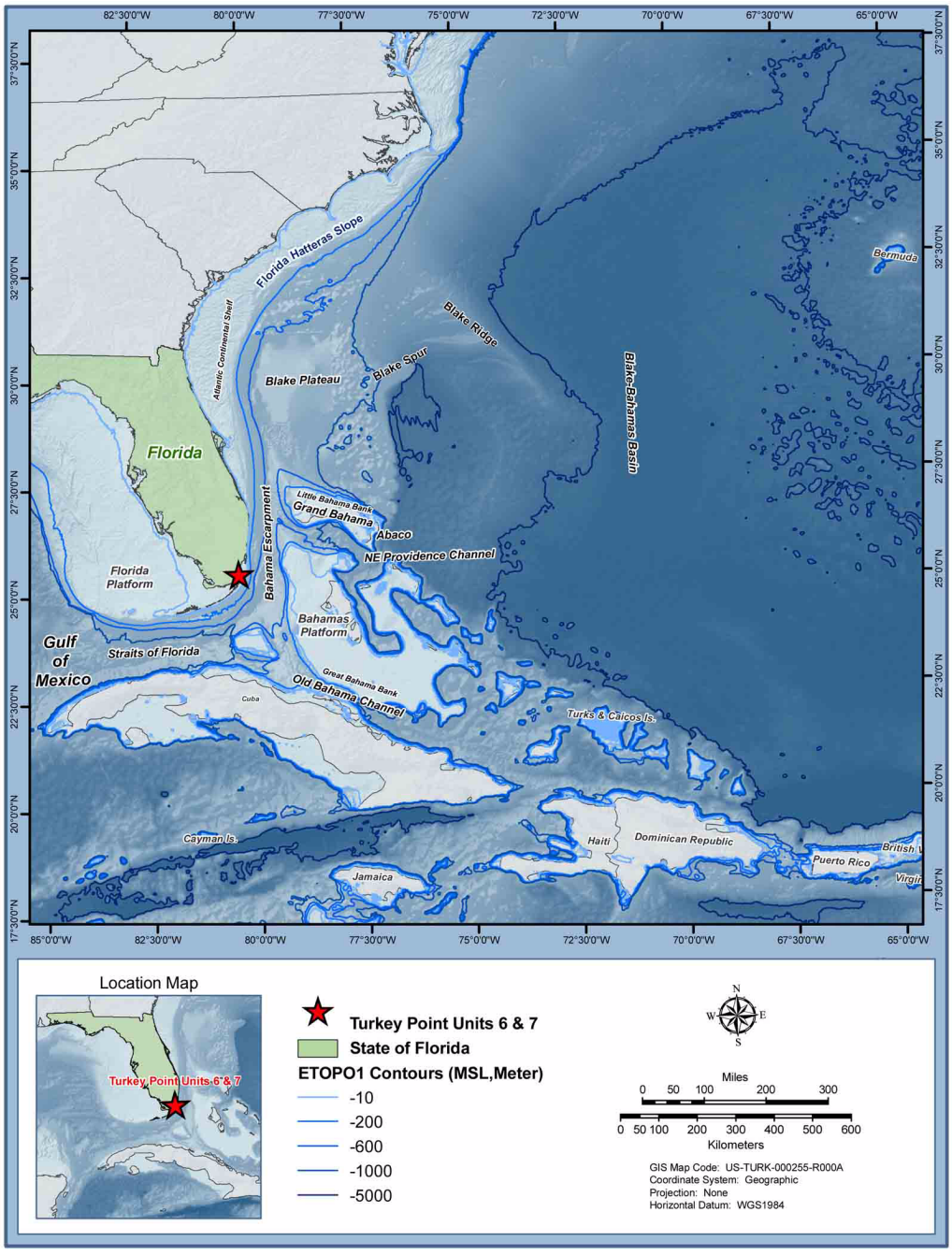

Figure 2.4.6-210 Extent of Selected Tsunami Model Domain and Subdomains SITE, ISLANDS, and DEEP

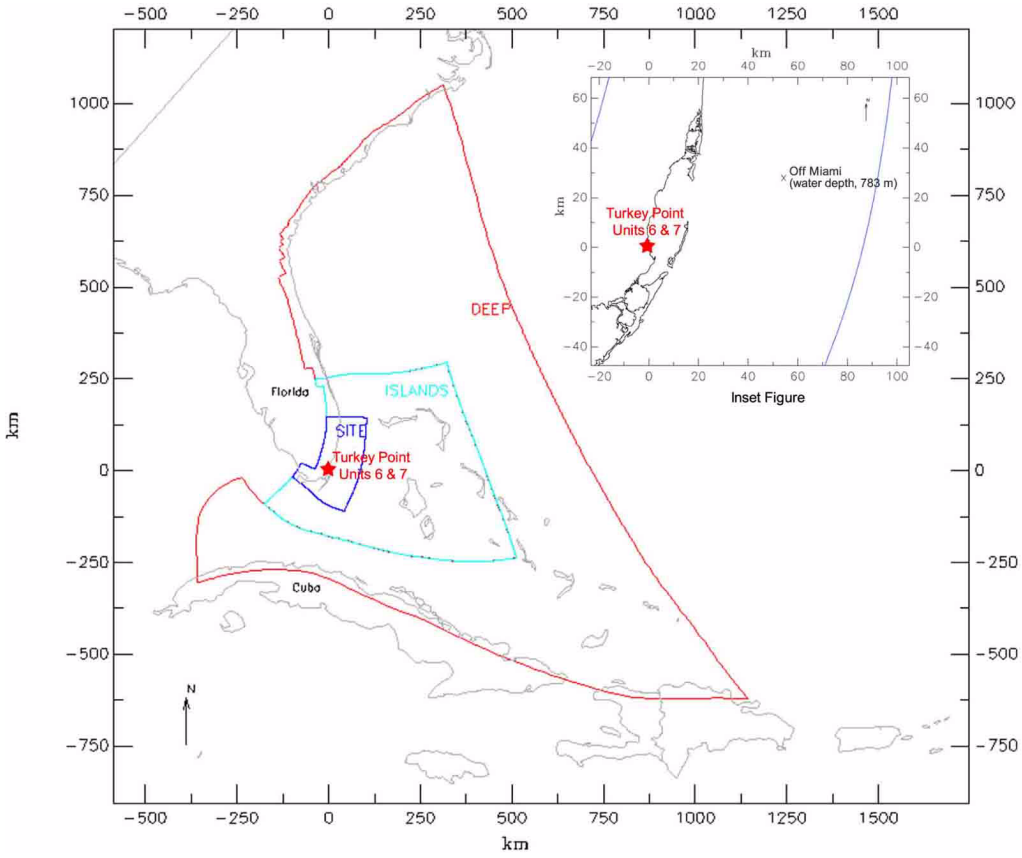

Figure 2.4.6-211 Model Grids of the DEEP Subdomain

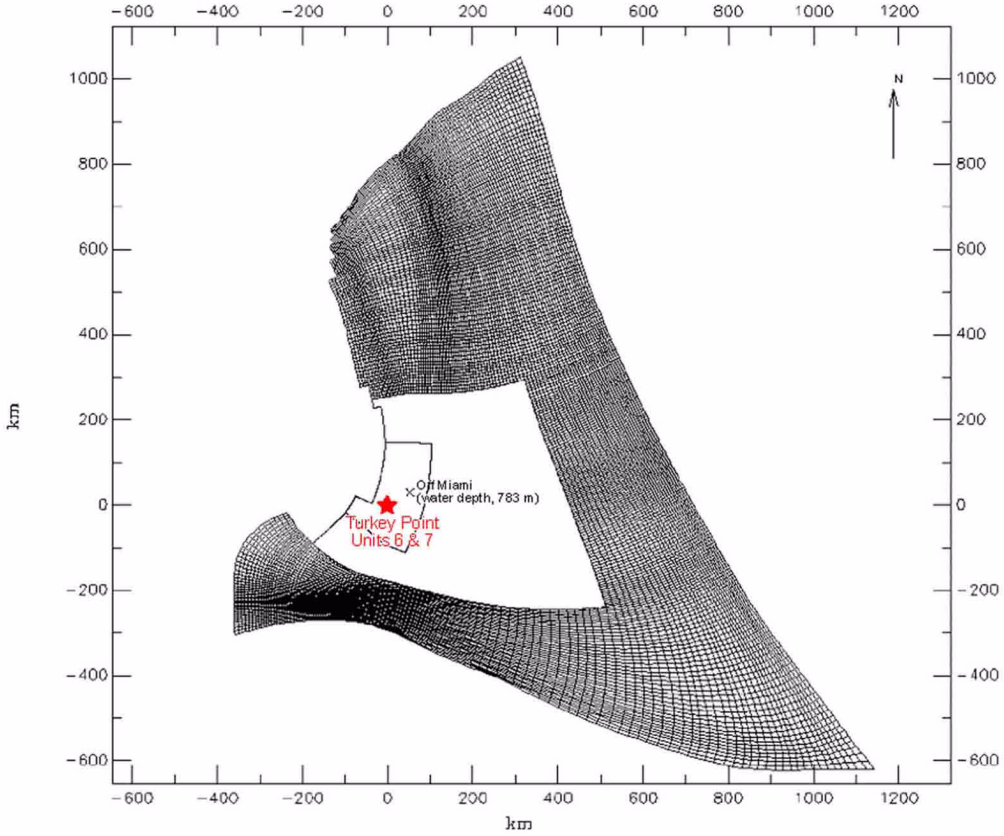

Figure 2.4.6-212 Model Grids of the ISLANDS Subdomain

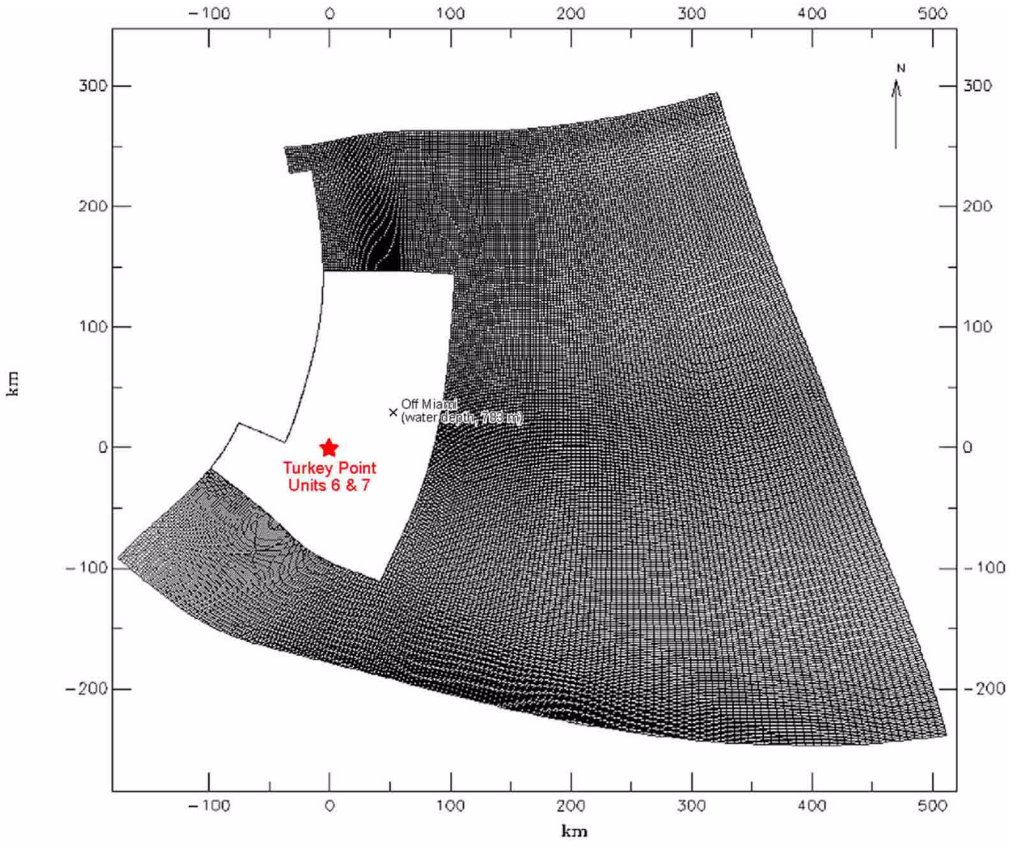

Figure 2.4.6-213 Model Grids of the SITE Subdomain near Units 6 & 7

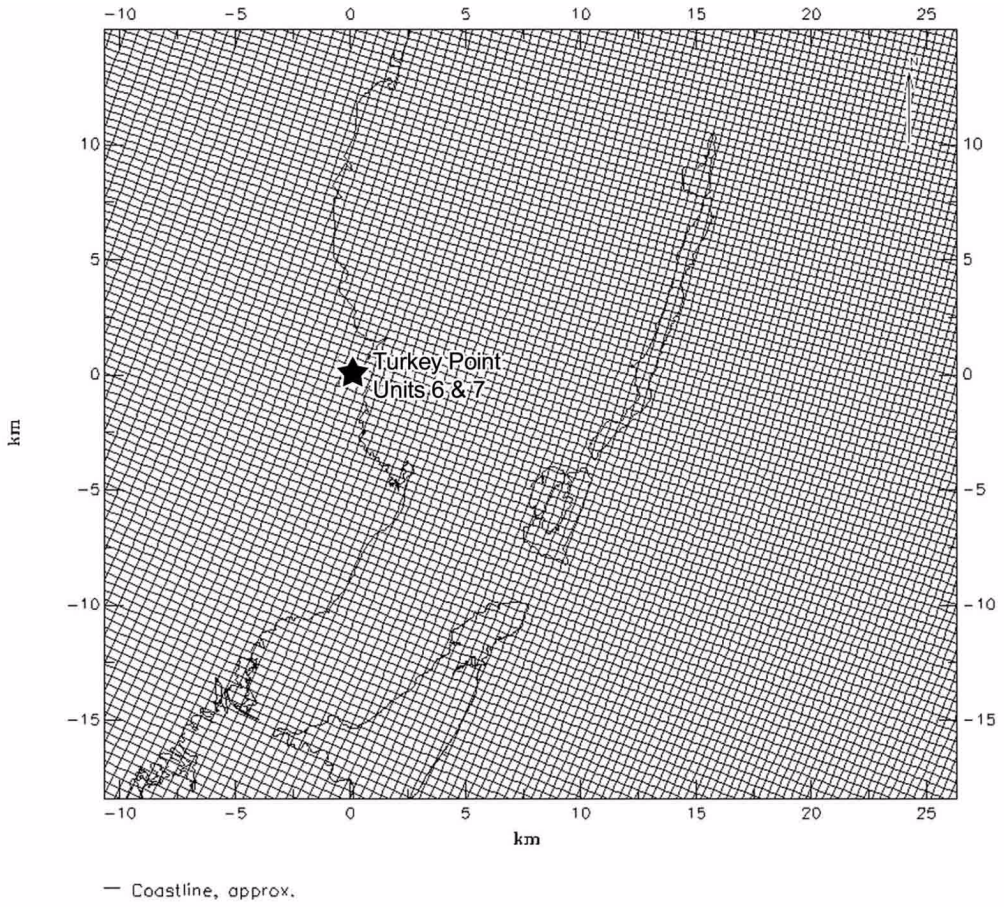

Figure 2.4.6-214 Contours of Model Bathymetry

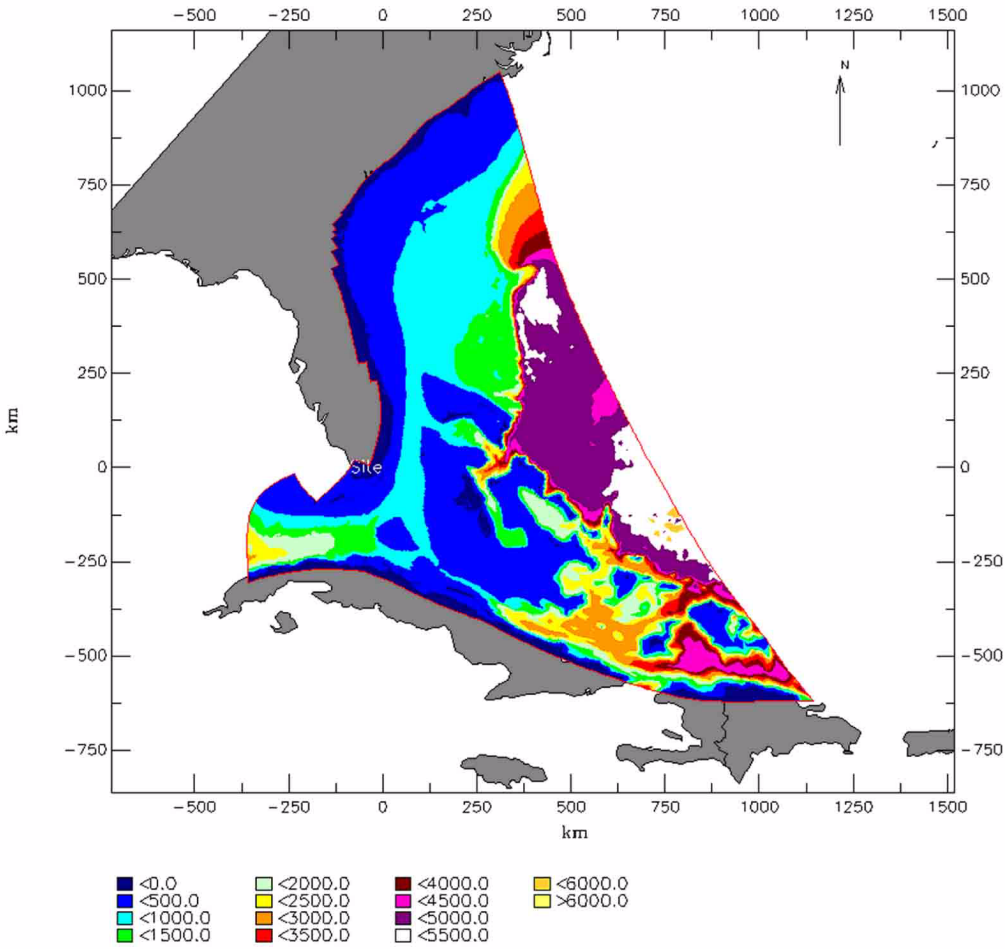

Note: Depths to the seabed are in meters relative to MSL

Figure 2.4.6-215 Postulated Epicenter Locations for the 1755 Lisbon Earthquake by AGMTHAG

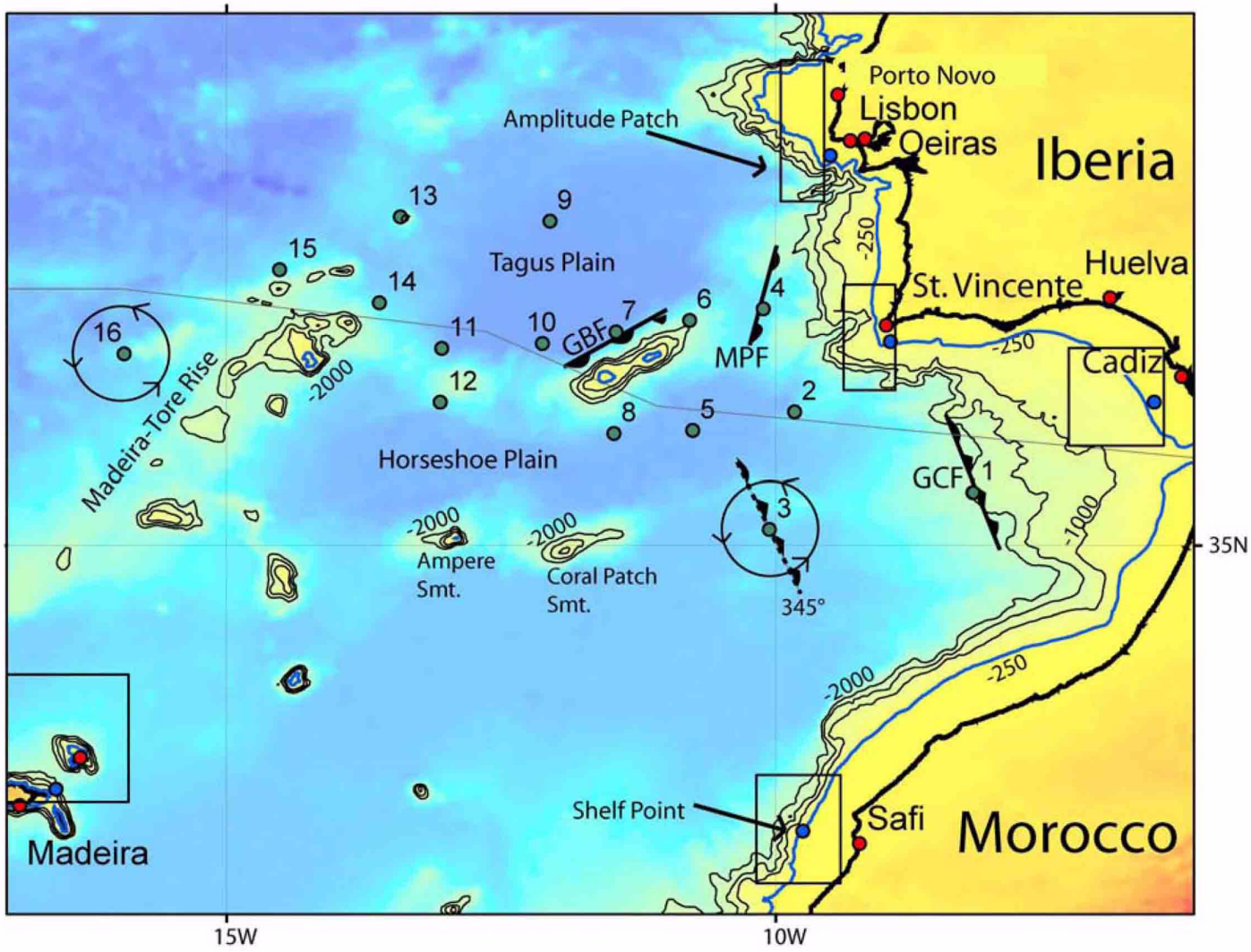

Note: Fault orientation for source locations 3 and 16 were rotated 360° at 15° to test the optimal strike angle generating maximum tsunami amplitude in the Caribbean. Depth contours are in meters.
Source: Reference 202

Figure 2.4.6-216 Input Tsunami Marigrams at the Model Open Boundary for Conditions with Single Wave, Continuous Wave Train, and Two Consecutive Waves

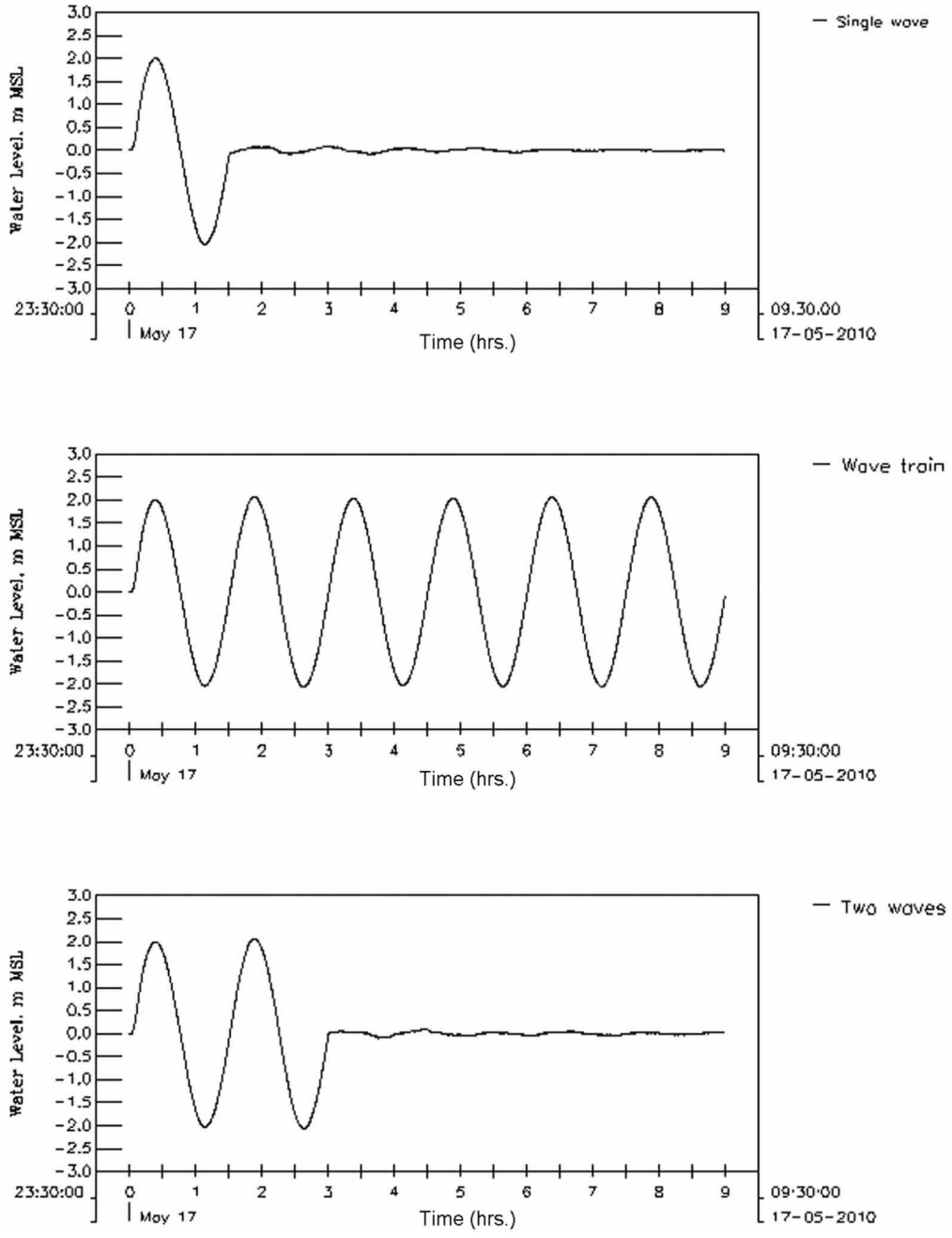

Figure 2.4.6-217 Simulated Tsunami Marigrams at 783 meters (2569 feet) Water Depth off Miami, Florida

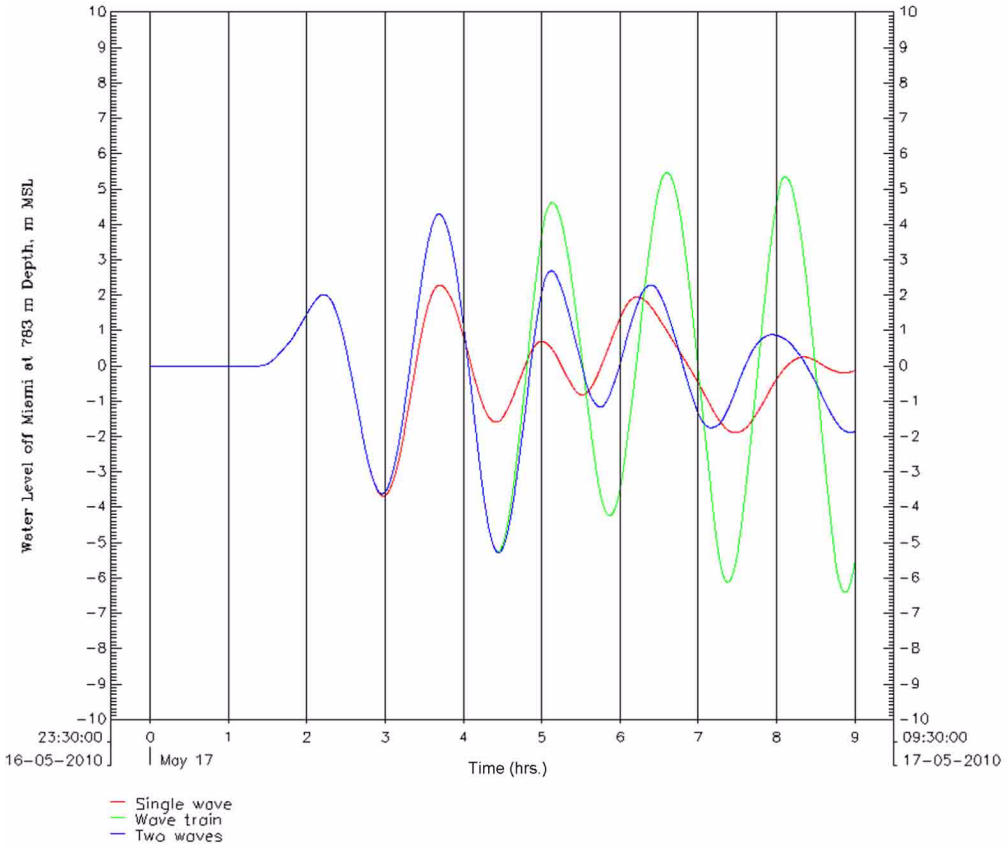

Note: Initial water level at MSL.

Figure 2.4.6-218 Simulated Tsunami Water Levels at the Units 6 & 7 Site for the Selected (Baseline) and Finer Grid Sizes

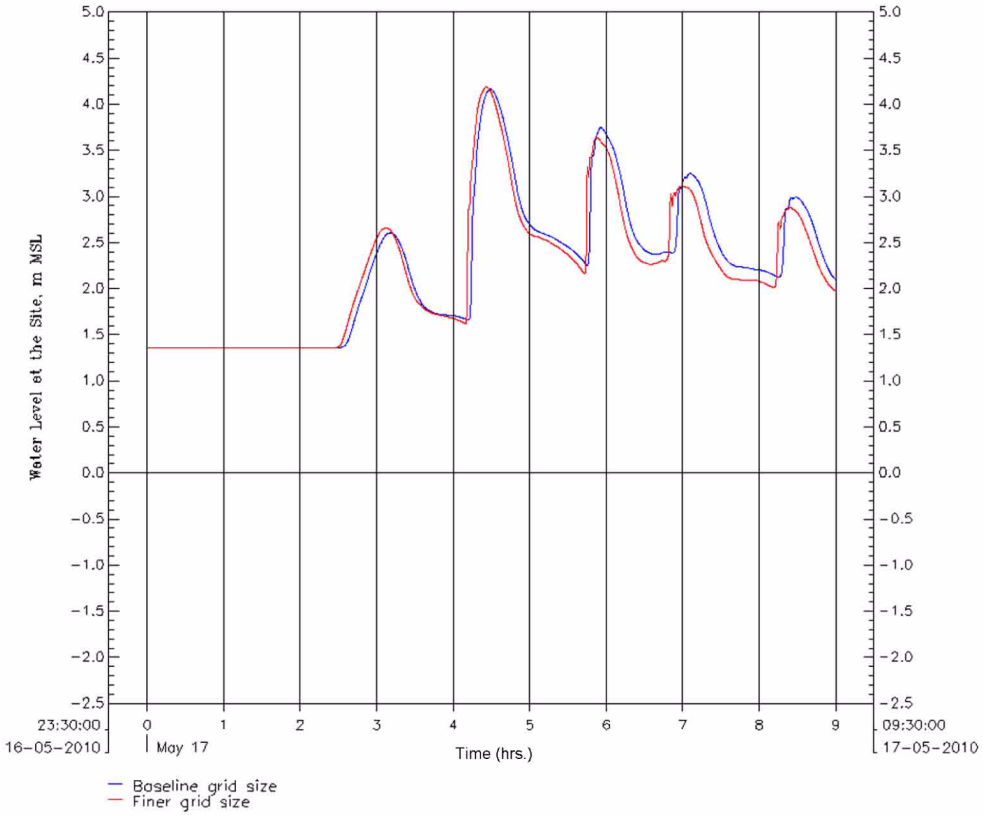

Note: Initial water level at 1.36 meters (4.46 feet) MSL.

Figure 2.4.6-219a Tsunami Water Level Contours 30 Minutes into the Model Simulation

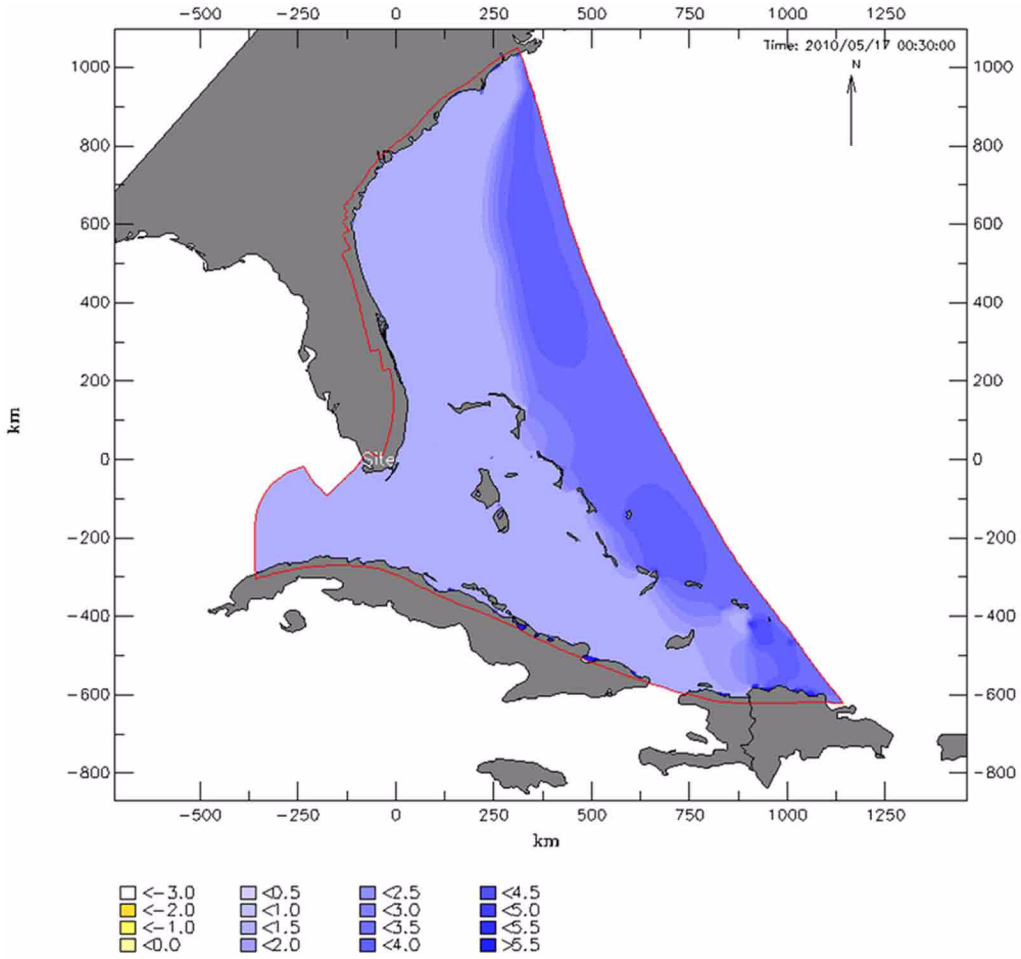

Note: Water levels are in meters MSL.

Figure 2.4.6-219b Tsunami Water Level Contours 1.0 Hour into the Model Simulation

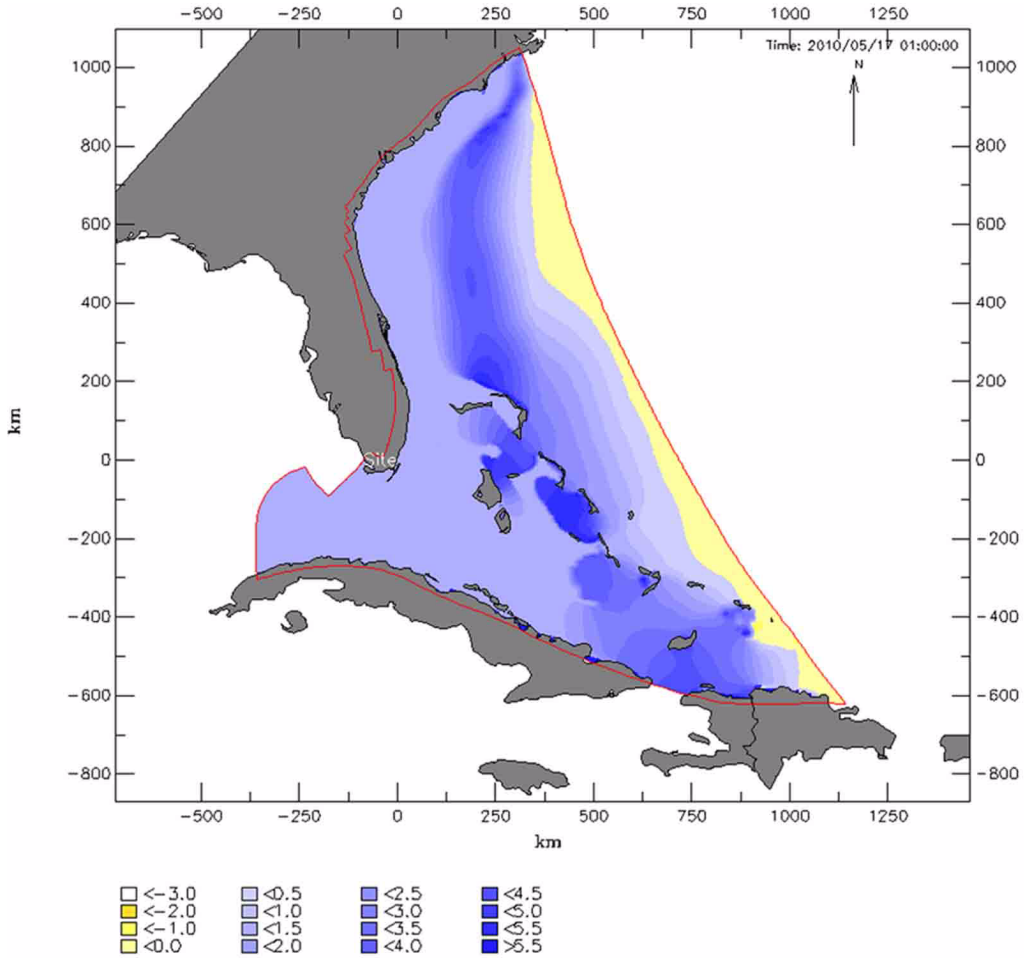

Note: Water levels are in meters MSL.

Figure 2.4.6-219c Tsunami Water Level Contours 1.5 Hours into the Model Simulation

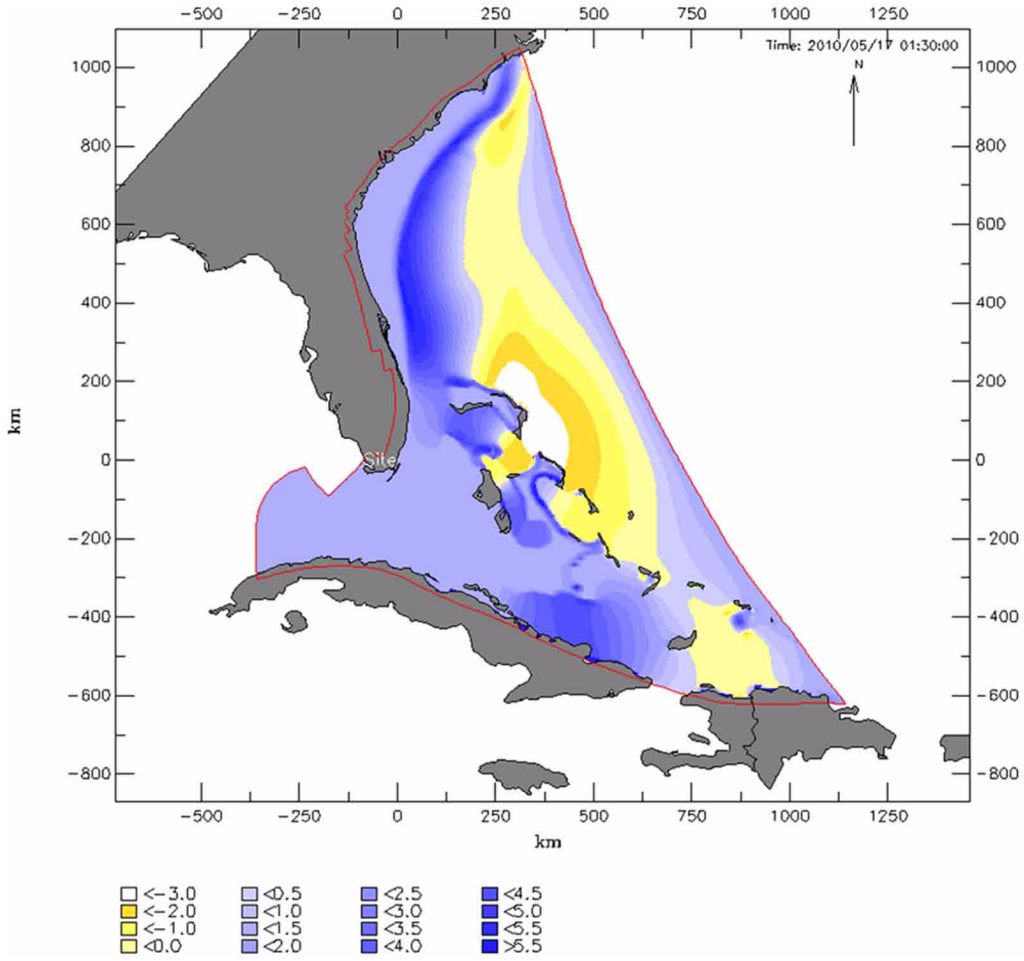

Note: Water levels are in meters MSL.

Figure 2.4.6-219d Tsunami Water Level Contours 2.0 Hours into the Model Simulation

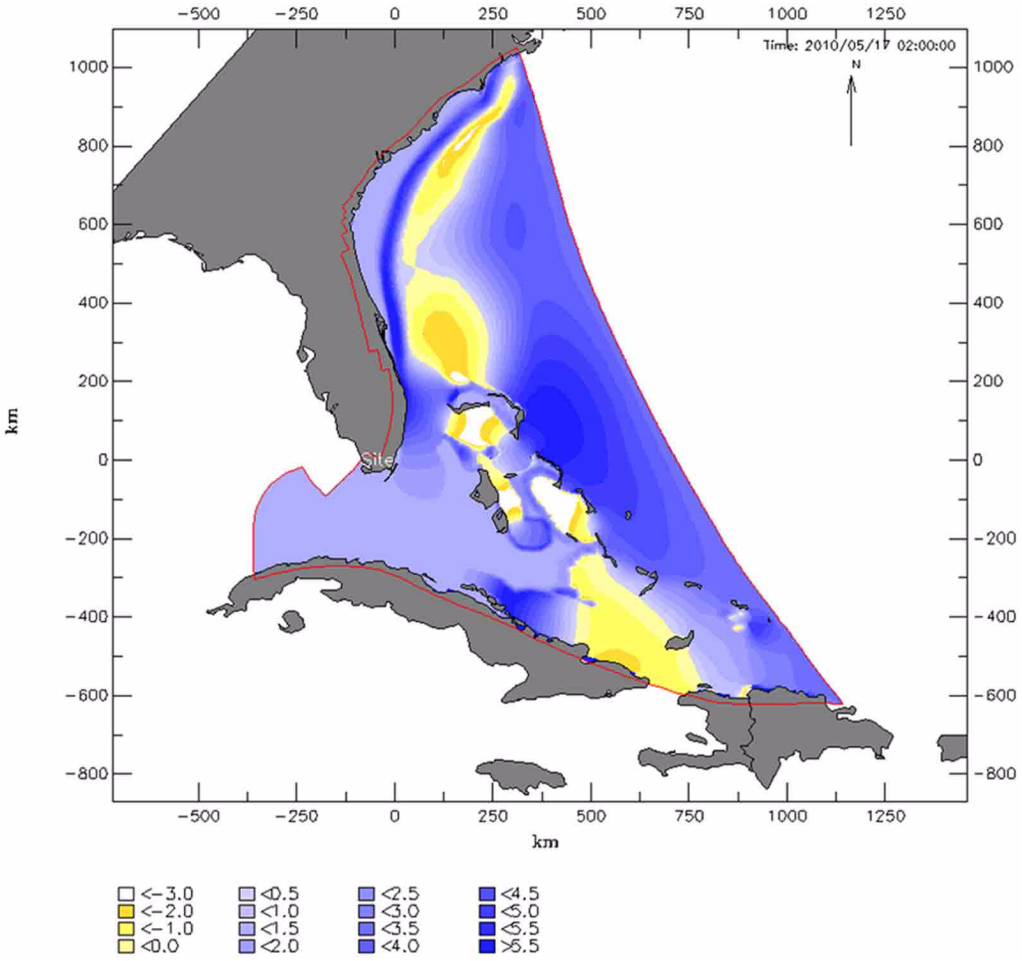

Note: Water levels are in meters MSL.

Figure 2.4.6-219e Tsunami Water Level Contours 2.5 Hours into the Model Simulation

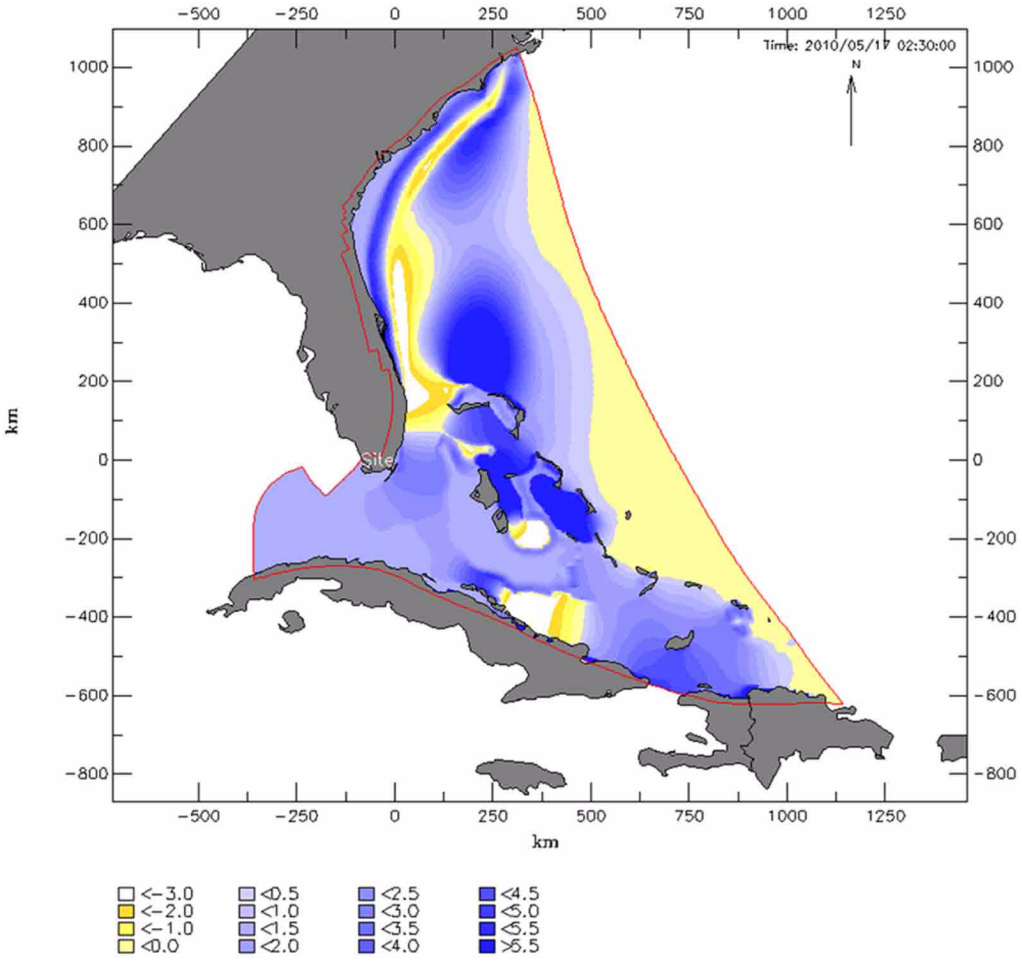

Note: Water levels are in meters MSL.

Figure 2.4.6-219f Tsunami Water Level Contours 3.0 Hours into the Model Simulation

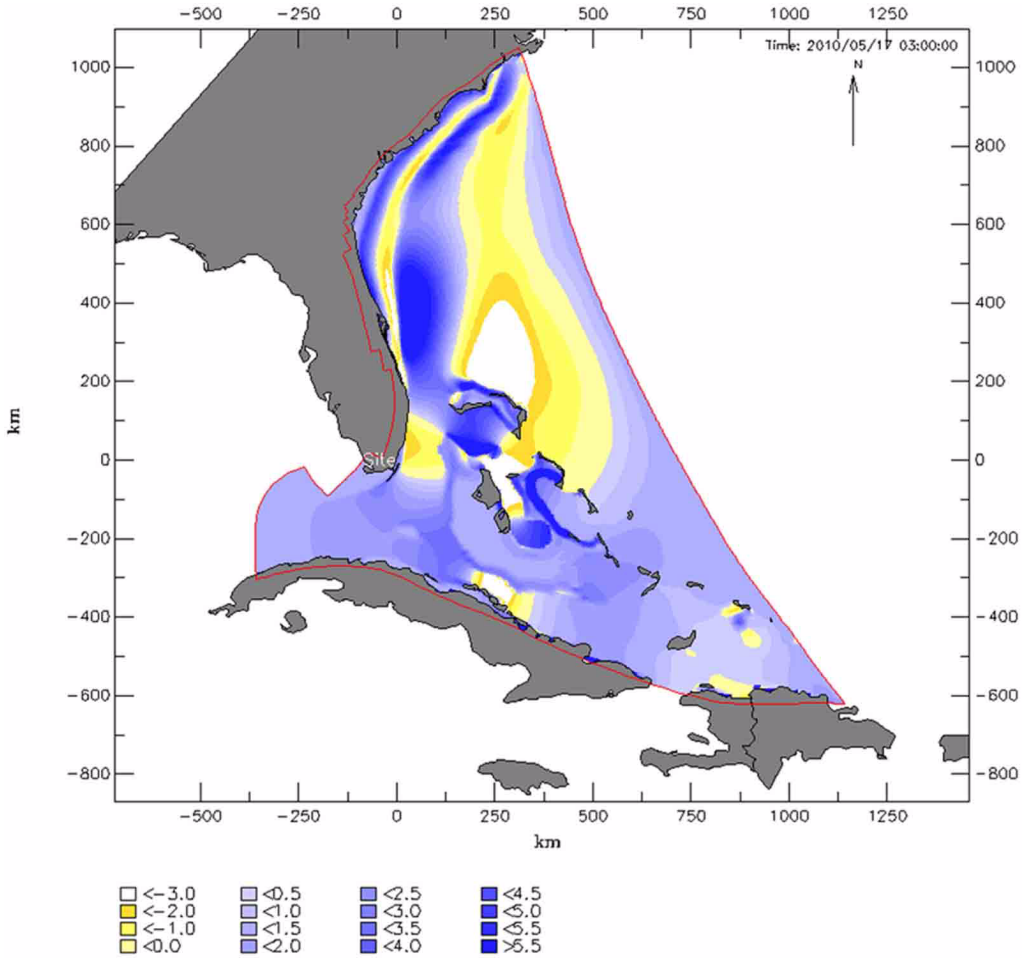

Note: Water levels are in meters MSL.

Figure 2.4.6-219g Tsunami Water Level Contours 3.5 Hours into the Model Simulation

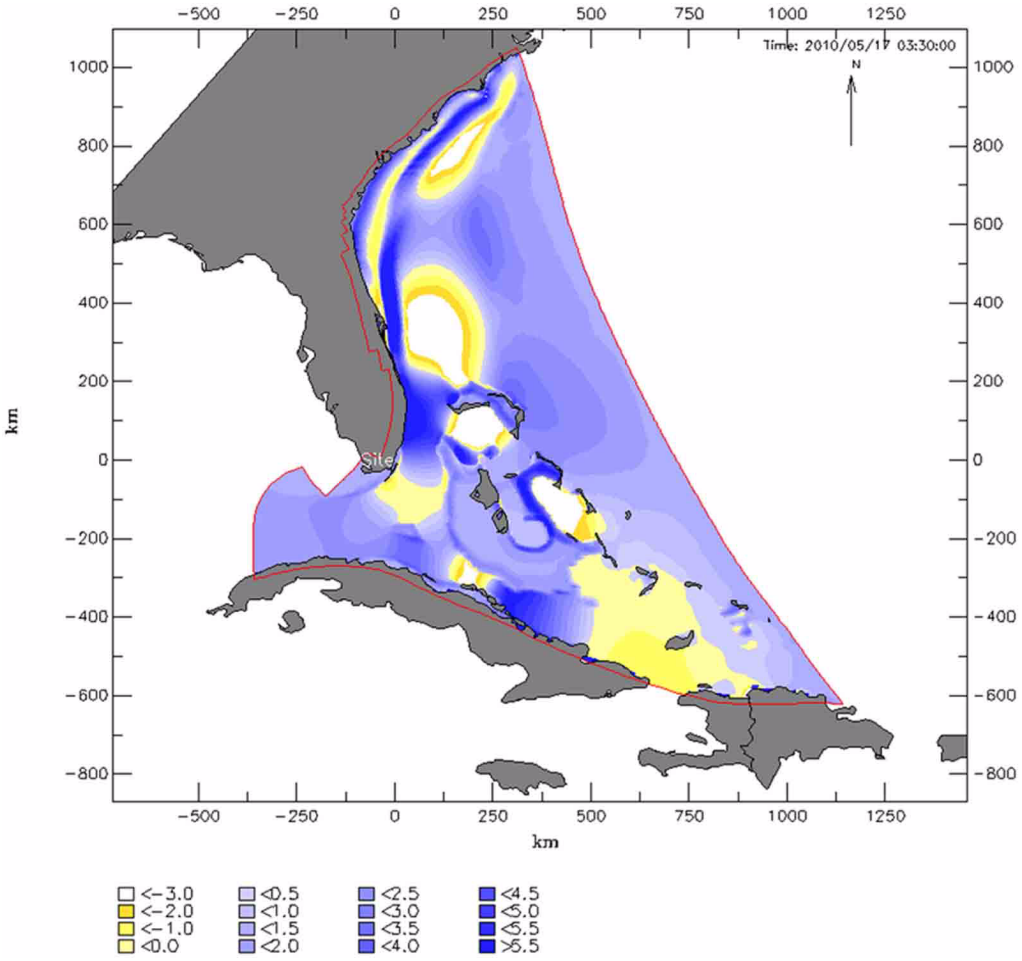

Note: Water levels are in meters MSL.

Figure 2.4.6-219h Tsunami Water Level Contours 4.0 Hours into the Model Simulation

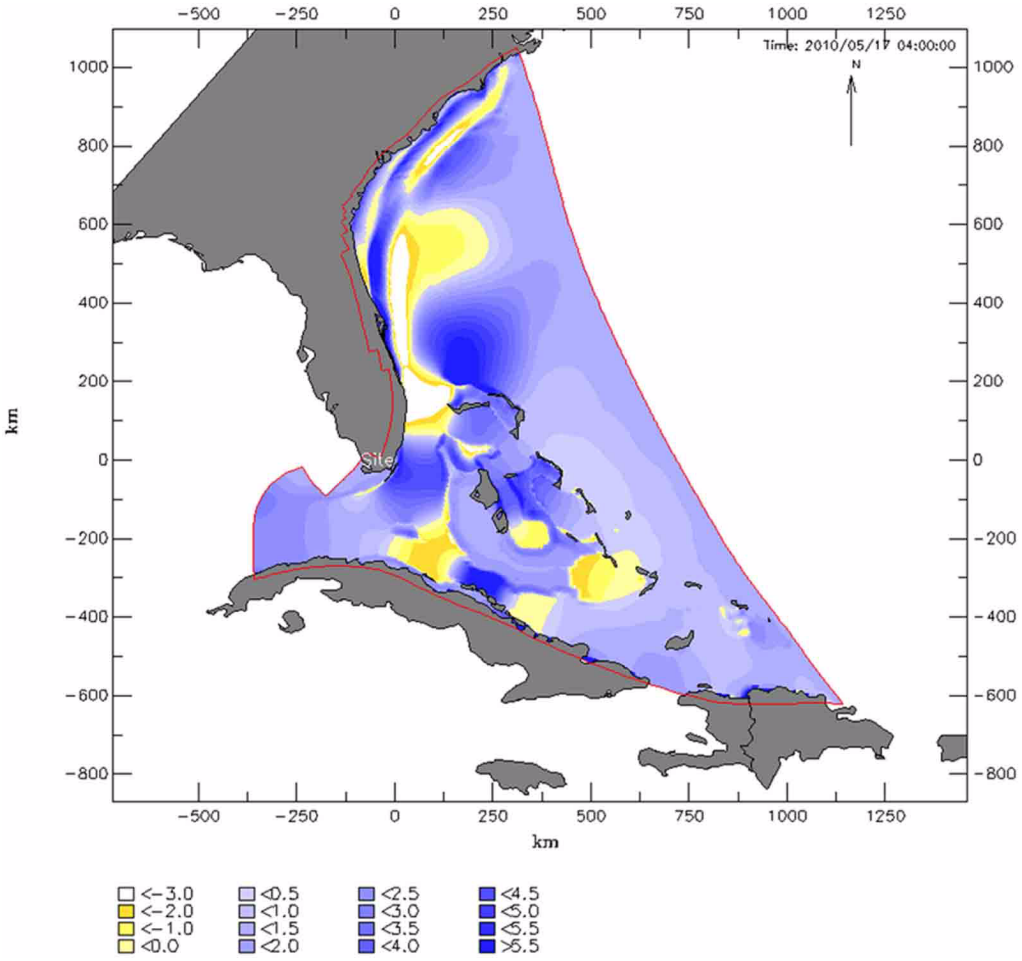

Note: Water levels are in meters MSL.

Figure 2.4.6-219i Tsunami Water Level Contours 4.5 Hours into the Model Simulation

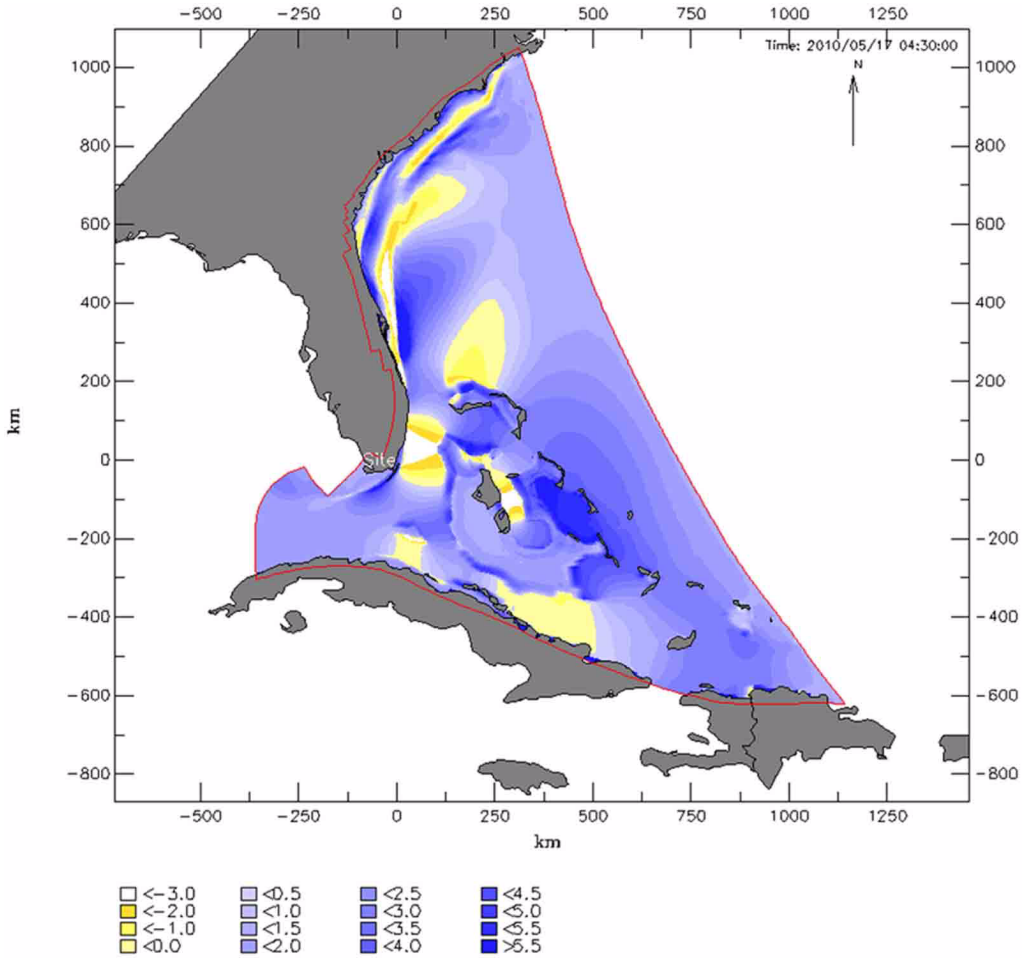

Note: Water levels are in meters MSL.

Figure 2.4.6-220 Tsunami Water Level Contours near the Units 6 & 7 Site 4.5 Hours into the Model Simulation Corresponding to the Time Close to the Maximum Water Level at Site

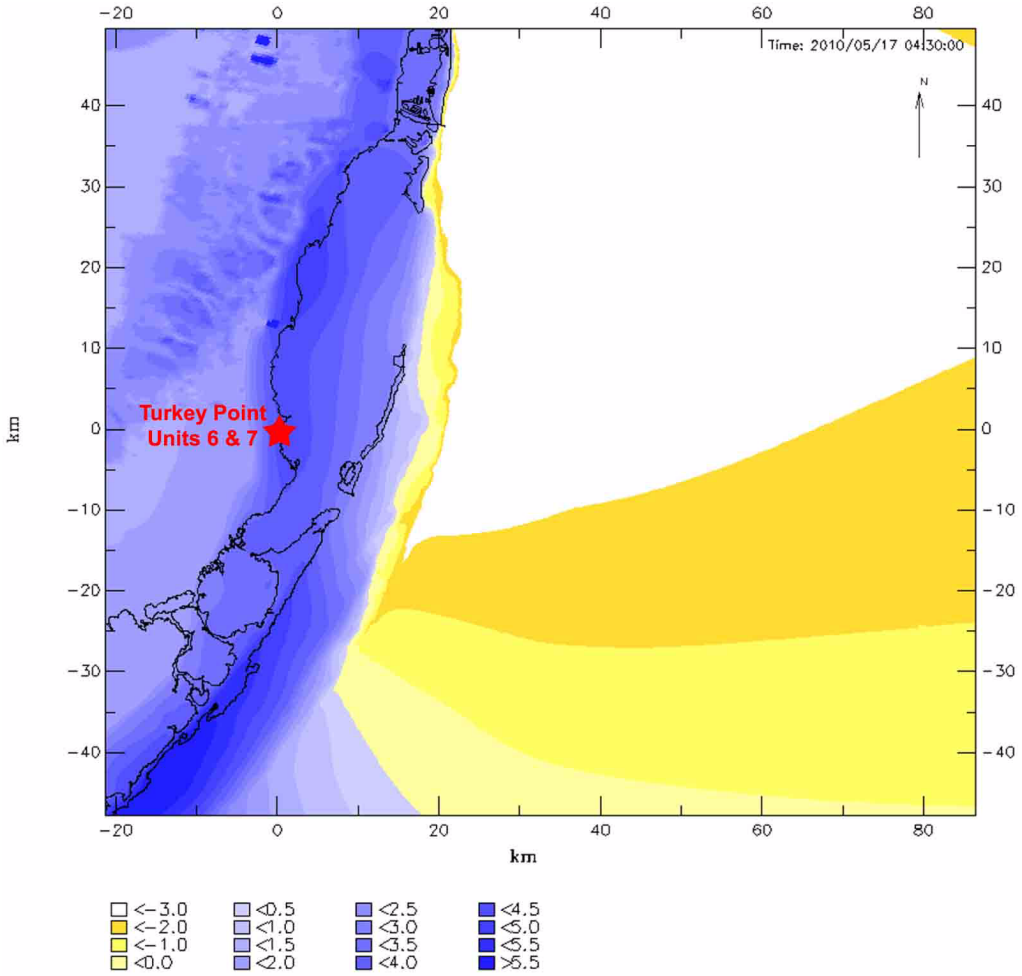

Note: Water levels are in meters MSL; some (dry) land elevations are shown as flood water levels according to designation in Delft3D-Flow.

Figure 2.4.6-221a Location of Simulated Water Level Monitoring Points along Track 1

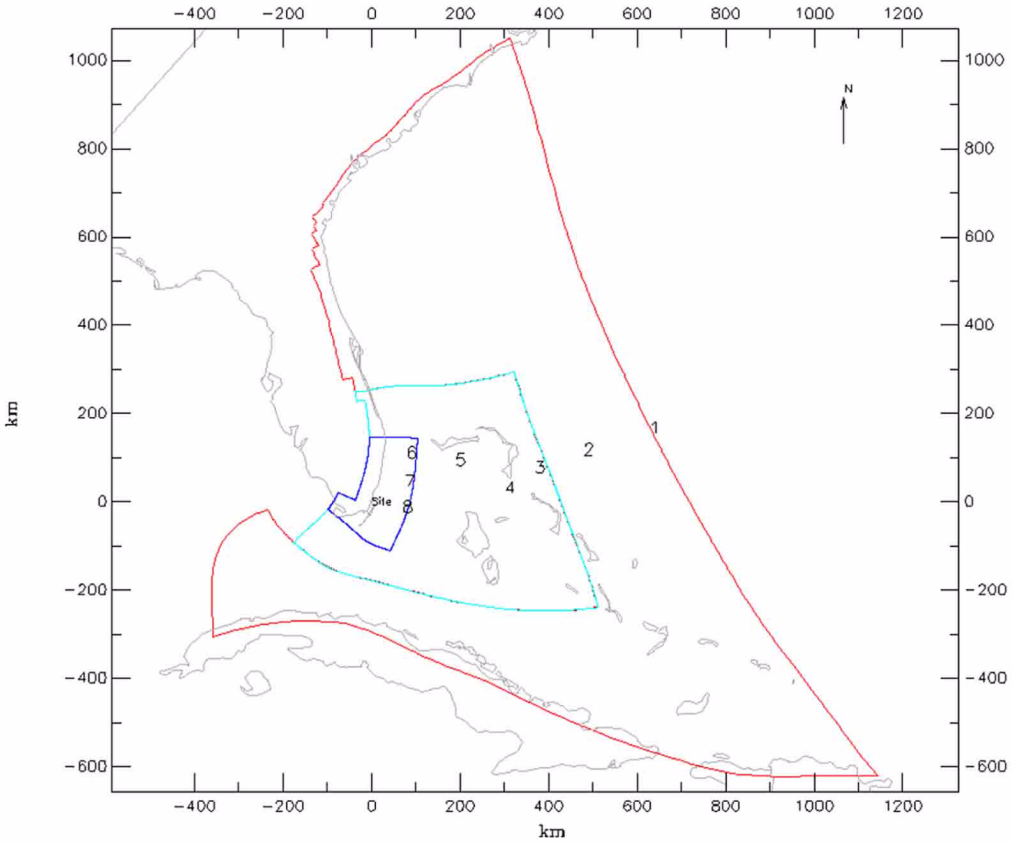

Figure 2.4.6-221b Location of Simulated Water Level Monitoring Points along Track 2

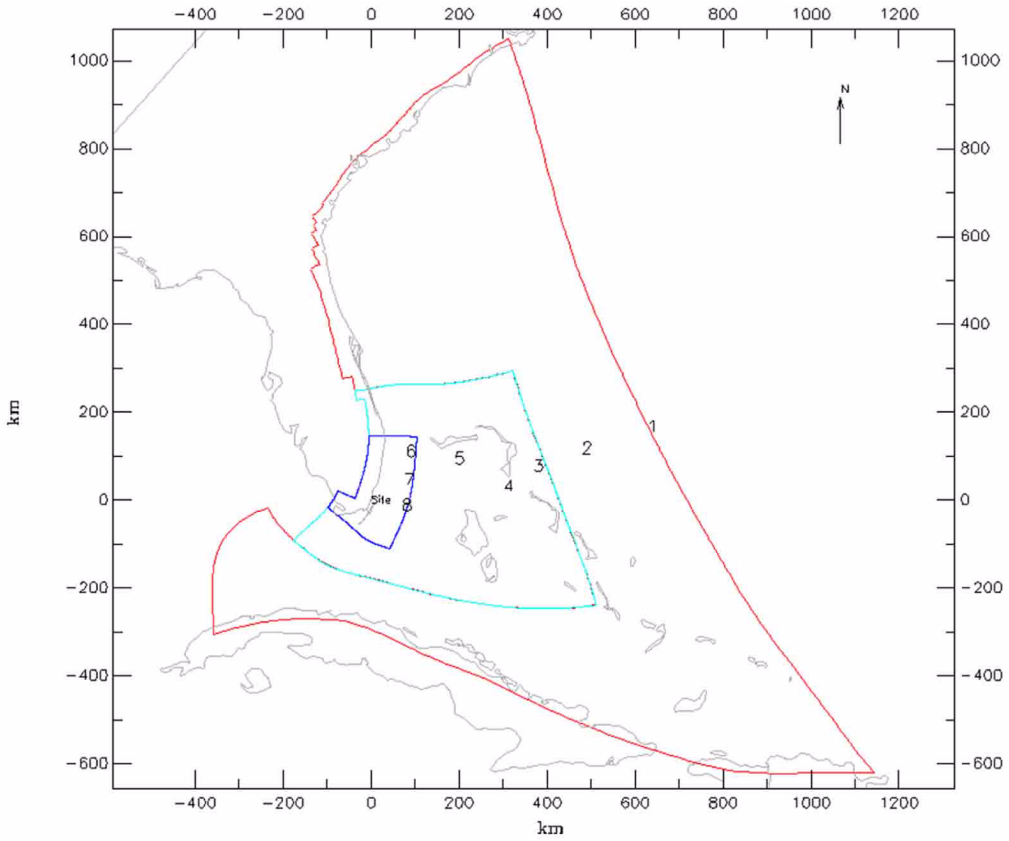

Figure 2.4.6-221c Location of Simulated Water Level Monitoring Points along Track 3

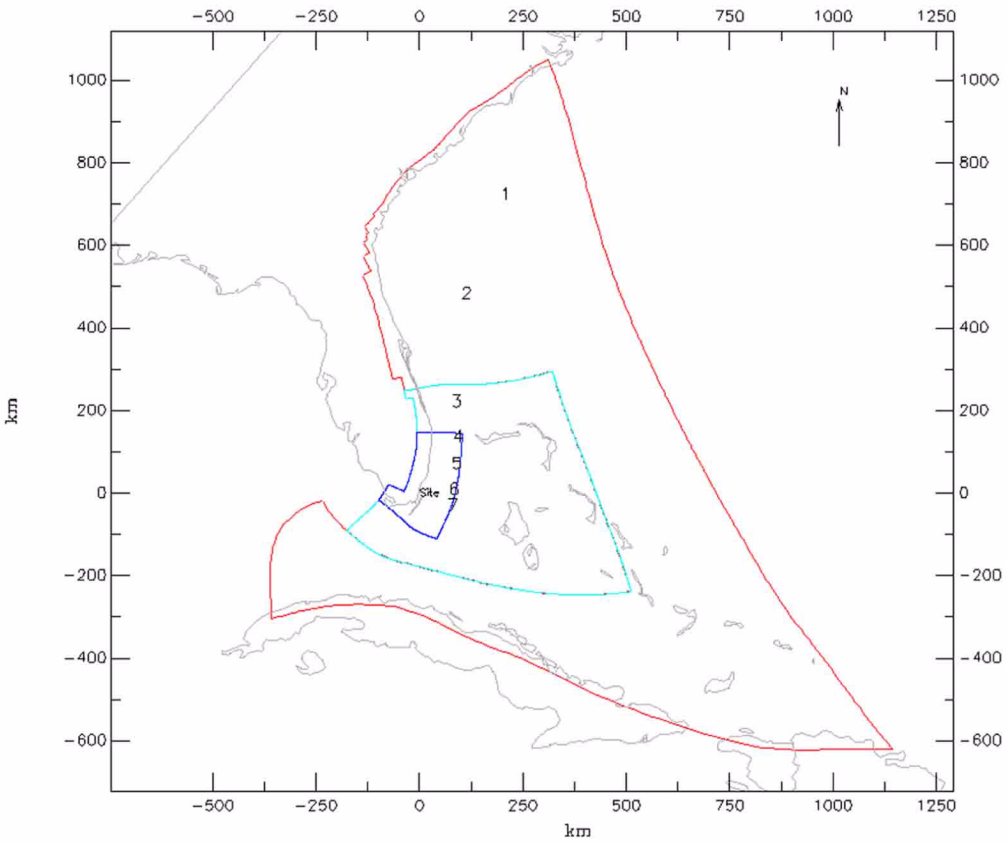

Figure 2.4.6-221d Location of Simulated Water Level Monitoring Points in Biscayne Bay and Vicinity (along with water depth contours)

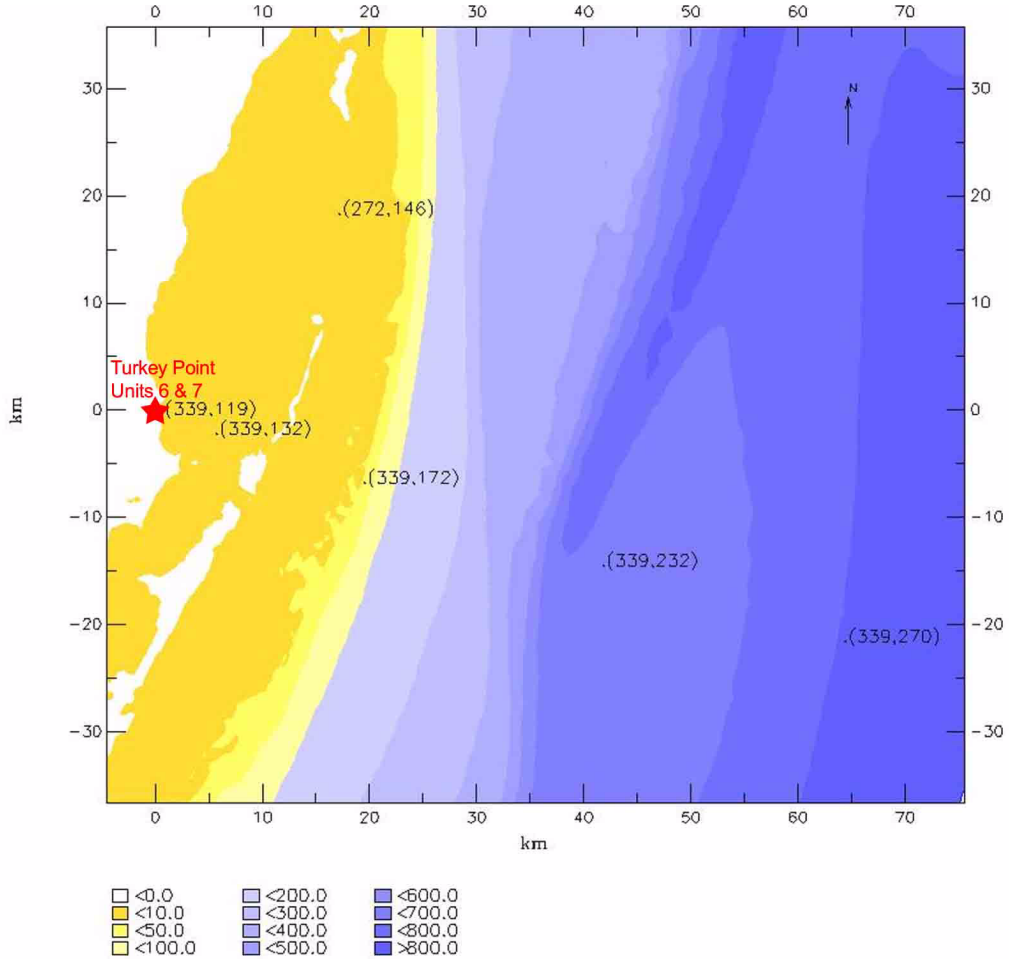

Note: Depths to the seabed are in meters relative to MSL.

Figure 2.4.6-222 Tsunami Marigrams at Monitoring Points along Track 1

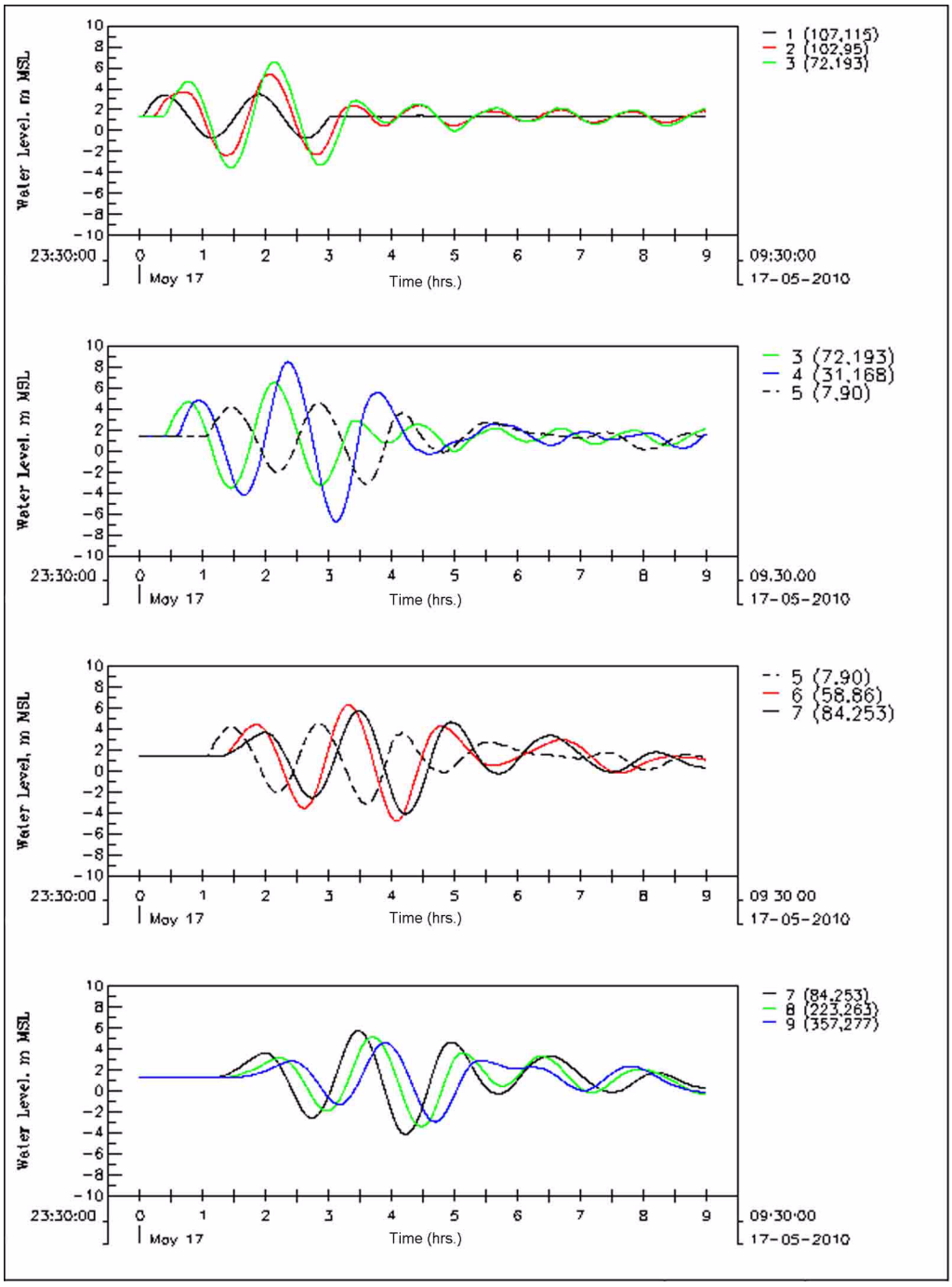

Figure 2.4.6-223 Tsunami Marigrams at Monitoring Points along Track 2

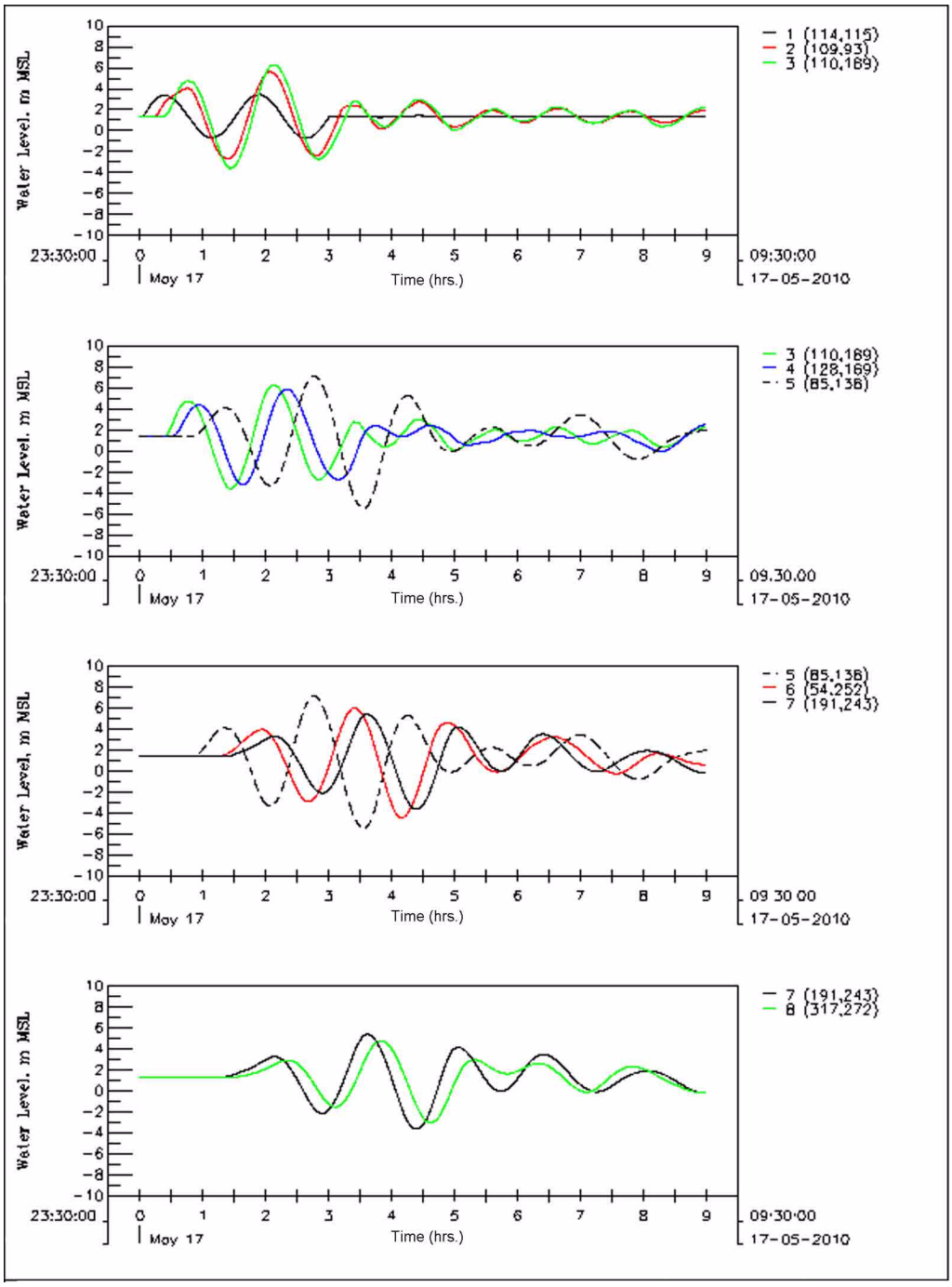

Figure 2.4.6-224 Tsunami Marigrams at Monitoring Points along Track 3

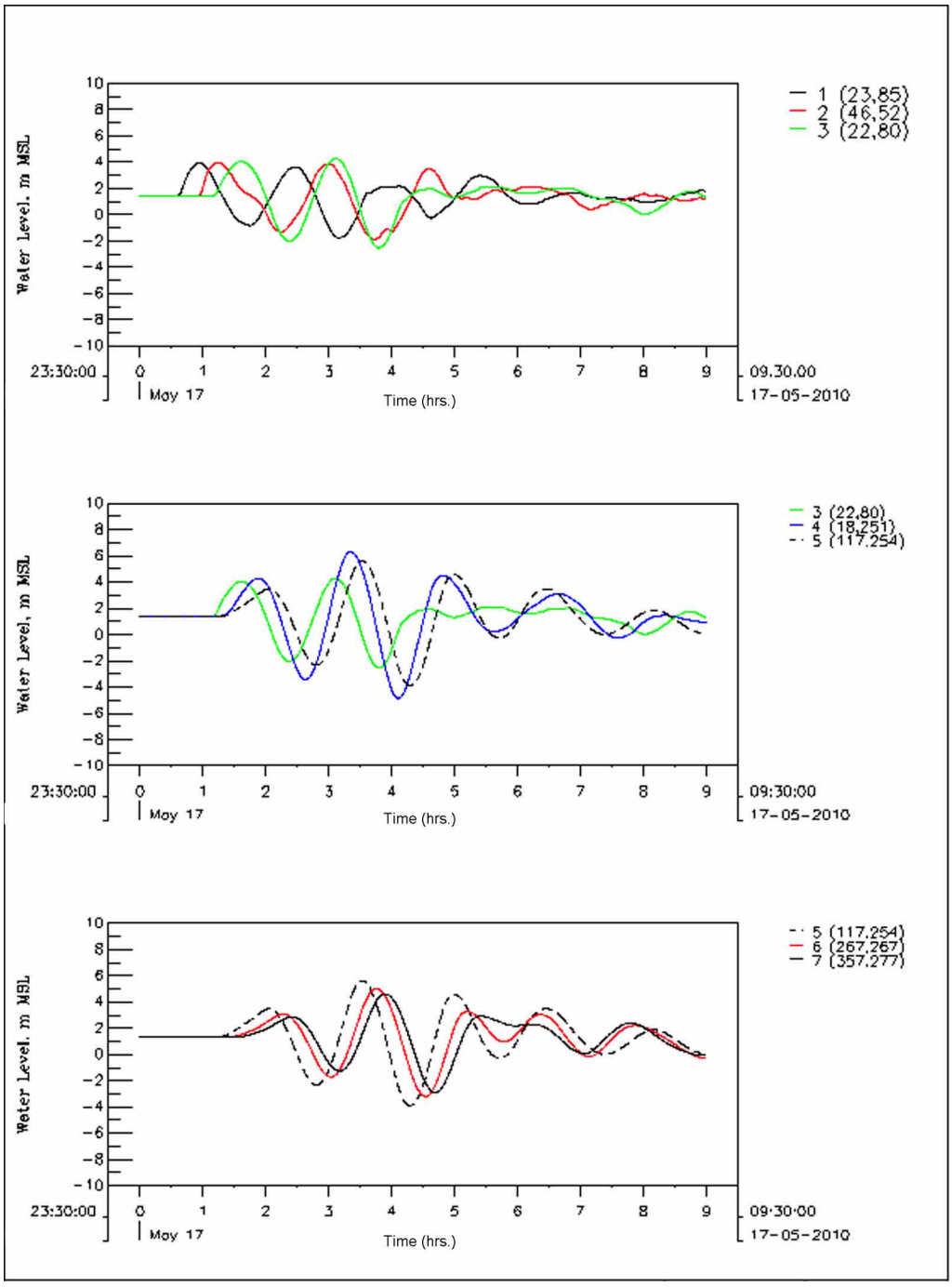

Figure 2.4.6-225 Tsunami Marigrams at Monitoring Points in Biscayne Bay and Vicinity

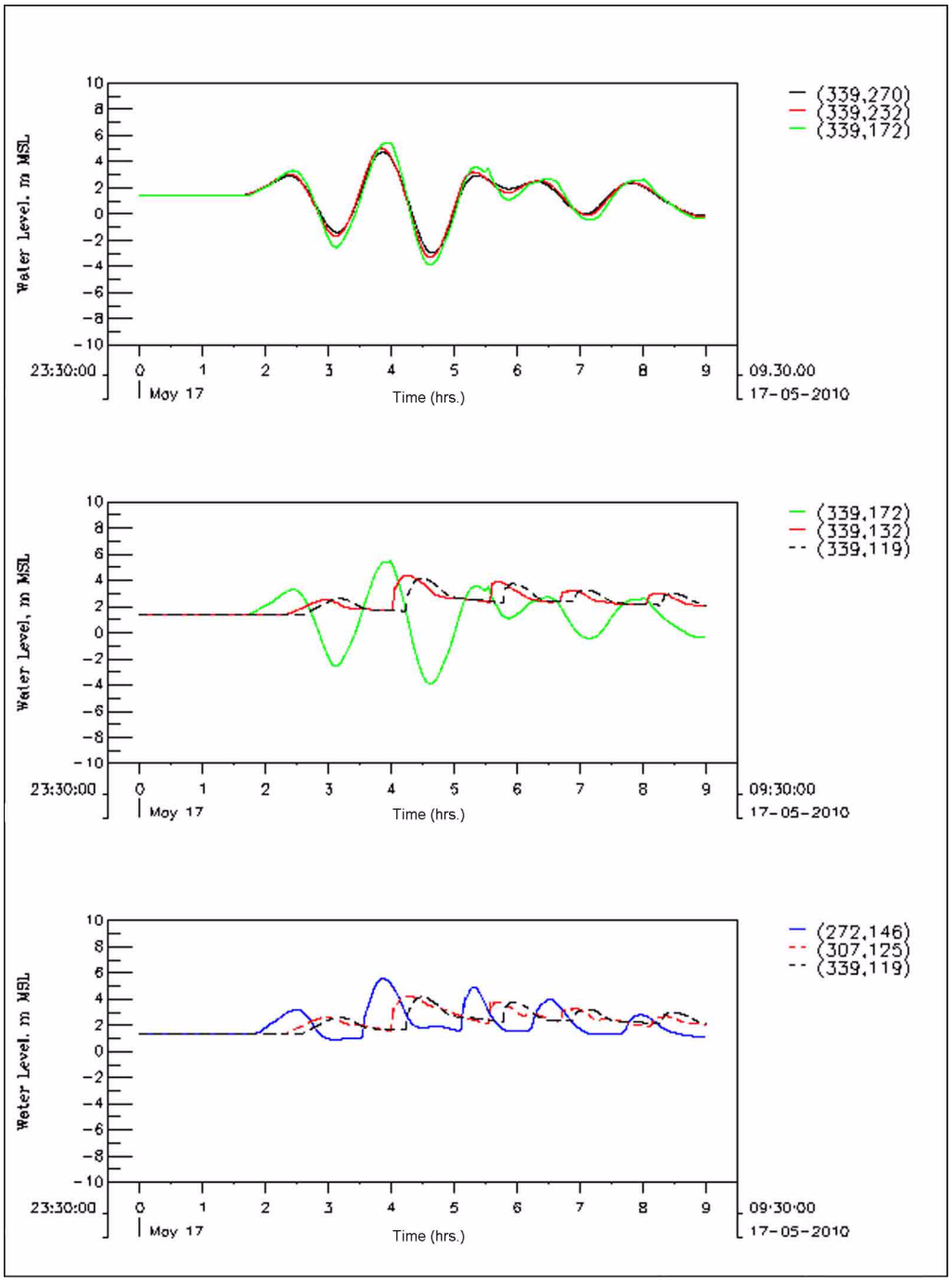

Figure 2.4.6-226 Simulated Tsunami Marigram at the Units 6 & 7 Site